



HAL
open science

The gp27-like Hub of VgrG Serves as Adaptor to Promote Hcp Tube Assembly

Melvin G Renault, Jordi Zamarreño Beas, Badreddine Douzi, Maïalène Chabalier, Abdelrahim Zoued, Yannick R Brunet, Christian Cambillau, Laure Journet, E. Cascales

► **To cite this version:**

Melvin G Renault, Jordi Zamarreño Beas, Badreddine Douzi, Maïalène Chabalier, Abdelrahim Zoued, et al.. The gp27-like Hub of VgrG Serves as Adaptor to Promote Hcp Tube Assembly. *Journal of Molecular Biology*, 2018, 430 (18 Pt B), pp.3143-3156. 10.1016/j.jmb.2018.07.018 . hal-01847145

HAL Id: hal-01847145

<https://amu.hal.science/hal-01847145>

Submitted on 23 Jul 2018

HAL is a multi-disciplinary open access archive for the deposit and dissemination of scientific research documents, whether they are published or not. The documents may come from teaching and research institutions in France or abroad, or from public or private research centers.

L'archive ouverte pluridisciplinaire **HAL**, est destinée au dépôt et à la diffusion de documents scientifiques de niveau recherche, publiés ou non, émanant des établissements d'enseignement et de recherche français ou étrangers, des laboratoires publics ou privés.

1 **ABSTRACT**

2

3 **Contractile injection systems are multiprotein complexes that use a spring-like**
4 **mechanism to deliver effectors into target cells. In addition to using a conserved**
5 **mechanism, these complexes share a common core known as the tail. The tail comprises**
6 **an inner tube tipped by a spike, wrapped by a contractile sheath, and assembled onto a**
7 **baseplate. Here, using the Type VI secretion system (T6SS) as a model of contractile**
8 **injection systems, we provide molecular details on the interaction between the inner**
9 **tube and the spike. Reconstitution into the *E. coli* heterologous host in absence of other**
10 **T6SS components and *in vitro* experiments demonstrated that the Hcp tube component**
11 **and the VgrG spike interact directly. VgrG deletion studies coupled to functional assays**
12 **showed that the N-terminal domain of VgrG is sufficient to interact with Hcp, to initiate**
13 **proper Hcp tube polymerization, and to promote sheath dynamics and Hcp release. The**
14 **interaction interface between Hcp and VgrG was then mapped using docking**
15 **simulations, mutagenesis and cysteine-mediated cross-links. Based on these results, we**
16 **propose a model in which the VgrG base serves as adaptor to recruit the first Hcp**
17 **hexamer and initiates inner tube polymerization.**

18

1 INTRODUCTION

2 The Type VI secretion system (T6SS) is a multiprotein machine, widespread in Proteobacteria
3 and responsible for the delivery of effectors into prokaryotic as well as eukaryotic target cells,
4 thus participating to interbacterial competition and pathogenesis [1-8]. The T6SS comprises a
5 trans-envelope complex constituted of the TssJ, TssL and TssM proteins [9-11]. This TssJLM
6 membrane complex serves as a docking station for a tail-like structure [11-15]. The T6SS tail-
7 like structure is structurally, evolutionarily and functionally related to the tail of contractile
8 injection systems (CIS), a broad family of machines that use a spring-like mechanism to
9 deliver macromolecules into target cells [16-21]. A number of CIS act as autonomous
10 machineries and are released in the external medium where they bind to specific receptors
11 located at the cell surface of target cells. These include the prototypical contractile
12 bacteriophages of the *Myoviridae* family that injects their genome into bacterial host cells,
13 and particles such as R-pyocins, anti-feeding prophages and *Photorhabdus* virulence cassettes
14 [22-25]. Other CIS act intracellularly and are oriented toward the cell exterior. These include
15 the *Pseudoalteromonas luteoviolacea* metamorphosis-associated and *Amoebophilus asiaticus*
16 contractile machines, as well as the T6SS [16, 19, 20, 26-28]. These CIS are responsible for
17 the delivery of effector proteins that stimulate the genetic program of eukaryotic cells to
18 induce morphogenesis, interfere with the cytoskeleton or the signalling pathway in eukaryotic
19 cells, or cause cell damages in bacterial cells [5, 6, 20, 26, 29, 30]. Hence, CIS participate to
20 establishment of symbiosis, pathogenesis, modification of the host or bacterial competition.
21 The mechanism of action is conserved between all these machines: a needle is propelled by
22 the contraction of a sheath and penetrates into the target cell to deliver macromolecules [28].
23 However, these systems have evolved additional modules to fulfil specific functions [21].
24 Extracellular CIS have fibers that mediate contact with the target cell by binding to specific
25 receptors. Intracellular CIS are anchored to the cell envelope by a membrane anchor or

1 membrane complex that orients the CIS toward the exterior and serves as channel for the
2 passage of the needle during sheath contraction [21]. At the molecular level, the CIS is
3 constituted of a needle surrounded by a contractile sheath and built on an assembly platform,
4 the baseplate [12, 22, 31, 32]. The needle is composed of an inner tube tipped by a puncturing
5 device [19, 22, 28]. The baseplate comprises conserved components that form wedges that
6 assemble around the central hub [12, 31, 33]. In most cases, the central hub connects the inner
7 tube with the puncturing device [34-36]. However, in T6SSs, the central hub and the
8 puncturing device are fused as a single polypeptide, a chimera protein called VgrG [1, 37, 38].
9 Hence it is predicted that VgrG represents both the central part of the baseplate and the tail
10 tube-puncturing device connector [31, 39, 40]. Indeed, interactions of VgrG with the inner
11 tube Hcp protein has been evidenced in *Agrobacterium tumefaciens* and with several
12 baseplate components including TssK and the TssFG complex in enteroaggregative
13 *Escherichia coli* (EAEC) [12, 41, 42]. The structure of the uropathogenic *E. coli* VgrG N-
14 terminal fragment corresponding to the hub has been solved [38], as well as the full-length
15 VgrG1 protein from *Pseudomonas aeruginosa* [43]. VgrG form trimers and is constituted of
16 several domains: (i) an N-terminal domain that resembles the bacteriophage T4 gp27 and
17 other phages hub proteins and that has, in the trimer, the overall structure of two
18 superimposed disks, (ii) an oligonucleotide/oligosaccharide-binding (OB)-fold domain which
19 is structurally similar to the bacteriophage T4 gp5 OB-fold domain, and (iii) the puncturing
20 device which is comparable to the membrane-penetrating gp5 triple-stranded β -helix [35, 37,
21 38, 43-45]. In addition to the core gp27-gp5 structure, additional domains could be found at
22 the VgrG C-terminal extremity, such as effector domains bearing an enzymatic activity or
23 adaptor domains that binds specific effectors [6, 7, 37, 46]. Therefore, T6SS-associated VgrG
24 proteins have a modular architecture and serve as hub for baseplate assembly, syringe for
25 target cell membrane penetration, docking site for effector translocation, and connector for

1 tail tube. In T6SS, the tail polymerizes once the baseplate docks to the membrane complex
2 [11, 12]. Assembly of the inner tube proceeds by the addition of Hcp hexameric rings that
3 stack on each other in a head-to-tail organization [47]. Hcp shares the same fold as tailed
4 phages major tail proteins that are structurally related to the upper ring domain of the phage
5 T4 gp27 hub [38, 44, 48, 49]. Polymerization of the sheath proceeds by the addition of TssBC
6 complexes at the distal end of the growing tail structure [19, 28, 50-52]. The assembly of the
7 tube is coordinated with that of the sheath: in absence of sheath, the Hcp hexameric rings do
8 not stack properly whereas no sheath extension occurs in absence of Hcp [47]. The
9 coordinated polymerization of the tail is mediated by TssA, a protein that associates to the
10 baseplate and then recruits and incorporates new tube and sheath blocks at the distal extremity
11 [53, 54]. However, it is not yet known how the first ring of Hcp is recruited to the baseplate
12 and how Hcp interacts with VgrG in the final needle structure. Interestingly, the N-terminal
13 disk of VgrG has a structure comparable to that of the hexameric Hcp, and therefore has been
14 proposed to connect the axial 6-fold symmetry of Hcp with the 3-fold axial symmetry of the
15 β -helix needle [38, 44]. VgrG therefore constitutes a good candidate to serve as nucleation
16 factor for the inner tube. Here, bacterial two-hybrid (BACTH) and co-immunoprecipitation
17 (co-IP) experiments show that VgrG1 interacts with Hcp1 in EAEC. Using shorter variants of
18 VgrG1, we provide evidence that the gp27-like hub domain of VgrG1 is sufficient to interact
19 with Hcp1, and that the strength of this interaction is comparable to that between Hcp1
20 hexamers. We then demonstrate that the VgrG hub domain is sufficient for the assembly and
21 the mechanism of action of the T6SS, as it promotes assembly of the inner tube and of the
22 contractile sheath, and permits Hcp1 release in the supernatant. Finally, targeted mutagenesis
23 and cysteine cross-linking studies reveal that the base of the VgrG1 gp27-like hub interacts
24 with the head surface of Hcp1. Taken together, these results allow to propose a model for the
25 assembly and the architecture of the hub/tube interface.

1

2 **RESULTS**

3 **VgrG1 interacts with Hcp1.**

4 To test whether VgrG and Hcp interact, the *vgrG* and *hcp* genes of the EAEC *sci-1* gene
5 cluster (*vgrG1*, EC042_4533, accession number (GI): 284924254; *hcp1*, EC042_4529, GI:
6 284924250) were cloned into BACTH vectors, in frame with the T18 and T25 domains of the
7 *Bordetella* adenylate cyclase, respectively. The results shown on reporter plates demonstrate
8 that Hcp1 and VgrG1 interact (Fig. 1A). The interaction between the two proteins was
9 confirmed by co-immunoprecipitation (co-IP) in the heterologous host *E. coli* K-12: VSV-G-
10 tagged VgrG1 specifically co-immunoprecipitated with FLAG-tagged Hcp1 (Fig. 1B and 1C).
11 These results show that the two proteins interact, and that this interaction is likely to be direct
12 because it occurs in the absence of the other T6SS genes in *E. coli* K-12.

13

14 **The VgrG1 N-terminal gp27-like hub is sufficient to mediate interaction with Hcp1.**

15 VgrG proteins form trimers with a modular architecture, as a result of fusion events between
16 gp27-like, gp5-like and adaptor/effector domains. In EAEC, the *Sci-1* VgrG protein, VgrG1,
17 is predicted to adopt a classic VgrG fold with the gp27-like hub and gp5 OB-fold and β -helix
18 domains. In addition, EAEC VgrG1 carries a C-terminal extension, comprising DUF2345 and
19 TTR domains, which binds to the Tle1 phospholipase effector [55]. To determine the region
20 of VgrG1 that interacts with Hcp1, we conducted a deletion mutagenesis coupled to co-IP
21 assays. First, VgrG1 boundaries were defined by modelling its structure based on the structure
22 of the *P. aeruginosa* VgrG1 protein (PDB: 4UHV; [43]): gp27-like hub (residues 1-386), gp5

1 OB-fold (residues 387-490), gp5 β -helix (residues 491-573), and C-terminal extension
2 (residues 574-841) (Fig. 2A and 2B). Fragments corresponding to the gp27-OB-gp5-C
3 (Δ DUF), gp27-OB (Δ gp5) and gp27 (Δ OB) regions (Fig. 2B) were fused to the VSV-G
4 epitope, and the interaction of the VgrG truncated variants with Hcp1 was assayed using co-
5 IP. Fig. 2C shows that none of the deletions affects the interaction with Hcp1, and hence that
6 the gp27-like hub domain is sufficient to promote VgrG1-Hcp1 complex formation. To
7 quantify the strength of this association, VgrG1- Δ OB and Hcp1 were purified. However,
8 while the isolated gp27 domain of VgrG1 was not stable, a variant comprising the OB fold
9 (*i.e.*, VgrG1- Δ gp5) was purified to homogeneity (Fig. 2D, left upper panel). The VgrG1- Δ gp5
10 interaction with Hcp1 was recorded by microscale thermophoresis (MST). VgrG1- Δ gp5 was
11 labelled with the amine-reactive blue fluorescent NHS dye and titrated against increasing
12 concentrations of Hcp1 (Fig. 2D, right upper panel). The fitted traces confirmed that VgrG1-
13 Δ gp5 interacts with Hcp1 with a K_D value of $\sim 2.8 \mu\text{M}$ (Fig. 2D, lower panel). Interestingly,
14 the VgrG-Hcp association is not restricted to the EAEC Sci-1 T6SS, as MST assays
15 demonstrated that (i) Hcp2, the Hcp protein encoded by the second T6SS gene cluster in the
16 EAEC 17-2 strain, interacts with its cognate VgrG, VgrG2- Δ gp5, with a K_D of $\sim 9.4 \mu\text{M}$ (Fig.
17 S1A), and (ii) the *V. cholerae* Hcp (Hcp_{Vc}) and VgrG (VgrG_{Vc}) interact with a K_D of ~ 4.1
18 μM (Fig. S1B). Hence, VgrG proteins interact with cognate Hcp proteins with an affinity in
19 the 1-10 μM range. To gain further information about the specificity of Hcp protein towards
20 VgrG, we performed cross-experiments where we tested the interaction of Hcp1 and Hcp2
21 with VgrG2- Δ gp5 and VgrG1- Δ gp5, respectively. MST results showed that VgrG1- Δ gp5 and
22 Hcp2 ($K_D \sim 35.5 \mu\text{M}$; Fig. S1C), and VgrG2- Δ gp5 and Hcp1 ($K_D \sim 22.4 \mu\text{M}$; Fig. S1D)
23 interact, although with lower affinity compared to the VgrG1- Δ gp5-Hcp1 and VgrG2- Δ gp5-
24 Hcp2 complexes. These results suggest that VgrG and Hcp proteins interact but that the
25 affinity is significantly higher between cognate pairs. However, *in vivo* interbacterial

1 competition assays showed that VgrG2 and Hcp2 are unable to compensate for the absence of
2 *vgrG1* and *hcp1*, respectively (Fig. S2). It is therefore unlikely that non-cognate VgrG and
3 Hcp proteins work together in EAEC cells.

4

5 **The VgrG1 gp27-like hub is sufficient to promote Hcp1 tube assembly, sheath dynamics**
6 **and Hcp1 release in the medium.**

7 T6SS biogenesis starts with the formation of the membrane complex and the recruitment of
8 the baseplate prior to coordinated assembly of the tail tube and sheath [11, 12, 53, 56]. Once
9 assembled, the T6SS sheath contracts and propels the Hcp tube toward the target cell to
10 deliver effectors [57]. A recent study has demonstrated that EAEC T6SS-mediated killing
11 requires the full-length VgrG protein, which comprises the C-terminal extension that binds
12 the Tle1 phospholipase effector [55]. However no information is available regarding the
13 contribution of VgrG1 domains for T6SS biogenesis. We thus tested whether VgrG1- Δ OB is
14 sufficient to promote tail tube and tail sheath assembly, and Hcp1 release in the medium (Fig.
15 3).

16 It has been proposed that assembly of the tail tube and sheath is concomitant, the
17 addition of a new Hcp ring immediately preceding the polymerization of a TssBC sheath
18 strand [47]. The arrangements of Hcp rings could be probed by disulfide bond formation
19 between cysteine side-chains located on each side of the Hcp ring [47, 58]. *In vivo*, Hcp1
20 rings organize in a head-to-tail manner with an estimated K_D of 7 μ M to form the tail tube
21 [59]. This organization is controlled by components of the baseplate, including VgrG1: in
22 their absence, Hcp1 rings associate randomly in head-to-tail, head-to-head and tail-to-tail
23 arrangements [12, 47]. We thus tested the minimal VgrG1 requirements for proper Hcp1 tube

1 assembly. Formation of disulfide bonds between pairs of cysteines that specifically report
2 head-to-head, tail-to-tail and head-to-tail Hcp1 assembly was tested in cells producing the
3 full-length VgrG1 or VgrG1 gp27-like hub (VgrG1- Δ OB). Cysteine-mediated cross-linking in
4 oxidative conditions showed that VgrG1- Δ OB is sufficient to control proper assembly of
5 Hcp1 tube exclusively in head-to-tail arrangements (Fig. 3A). Furthermore, dynamics of the
6 tail sheath could be observed by fluorescence microscopy using fluorescently-labelled TssB.
7 Time-lapse recordings show that the VgrG1- Δ OB construct is sufficient to mediate extension
8 and contraction of the T6SS tail sheath (Fig. 3B and Fig. S3). These results suggest that the
9 VgrG1 gp27-like hub is sufficient for proper assembly and action of the EAEC Sci-1 T6SS.
10 This hypothesis was confirmed by the observation that VgrG1- Δ OB is sufficient to enable
11 Hcp1 release in the milieu, a reporter of sheath contraction (Fig. 3C). The ability of VgrG1-
12 Δ OB to promote T6SS assembly is not due to the formation of functional heterologous
13 VgrG2/VgrG1- Δ OB trimer assemblies as production of VgrG1- Δ OB in *vgrG1-vgrG2* mutant
14 cells is sufficient to support Hcp release in the culture supernatant (Fig. S4).

15

16 **The head side of Hcp1 interacts with VgrG1.**

17 To define the side of Hcp1 that contacts VgrG1, we used tryptophan substitution
18 variants of Hcp1 previously described to prevent assembly of Hcp tubes by sterically
19 perturbing Hcp hexameric rings association [47, 59]. These tryptophan substitutions were
20 positioned at the head (S158W) or tail (N93W) side of Hcp1. Bacterial two-hybrid assays
21 showed that introduction of a tryptophan residue at position Ser-158 disrupts the interaction
22 with VgrG1 whereas a tryptophan at position Asn-93 does not impact Hcp1-VgrG1 complex
23 formation (Fig. 4A). The strong impact of the S158W mutation on VgrG1-Hcp1 complex
24 formation was further confirmed by co-immunoprecipitation (Fig. 4B). This result suggests

1 that the head side of Hcp1 contacts VgrG1 (Fig. 4C). The current model of EAEC T6SS
2 assembly proposes that TssA controls T6SS tail polymerization and binds to the distal end of
3 the tube/sheath during extension [53, 54]. This model implies that TssA should contact Hcp1
4 at the opposite side relative to VgrG1 (*i.e.*, the tail side). Bacterial two-hybrid experiments
5 using TssA and the Hcp1 tryptophan variants mirrored the VgrG1-Hcp1 interaction: the Hcp1
6 N93W variant does not interact with TssA whereas a tryptophan at position 158 does not
7 affect Hcp1-TssA interaction (Fig. 4A and 4B). Taken together, these results indicate that
8 TssA and VgrG1 bind to the two opposite sides of Hcp1: VgrG1 contacts the head side
9 whereas TssA interacts with the tail side (Fig. 4C).

10

11 **The VgrG1 loop 360-362 is required for VgrG1-Hcp1 complex formation.**

12 Because Hcp1 likely interacts with the basal side of the VgrG1 gp27-like domain, we
13 engineered a VgrG1 variant in which one of the protruding loops (Fig. 4C), comprising
14 residues Ser-360, Arg-361 and Lys-362, was exchanged by three glycine residues (S360G-
15 R361G-K362G; hereafter called VgrG1_{loop}). These mutations had no impact on VgrG1
16 multimer formation, as monitored by bacterial two-hybrid (Fig. 4D). However, protein-
17 protein interaction assays demonstrated that the VgrG1 360-362 region is important for
18 VgrG1-Hcp1 complex formation, as no interaction was detected between Hcp1 and VgrG1_{loop}
19 by bacterial two-hybrid and co-immunoprecipitation (Fig. 4B and 4D). Finally, production of
20 the VgrG1_{loop} variant does not compensate the absence of VgrG1 for *in vivo* Hcp1 tube
21 formation (Fig. 4E) and inter-bacterial activity (Fig. 4F). These results demonstrate that the
22 base of the VgrG1 hub-like domain, or at least the 360-362 loop, is critical for mediating
23 functional contacts with Hcp1.

1

2 **Disulfide bond formation identifies the T6SS hub-tube interface.**

3 To gain detailed insights onto the VgrG1-Hcp1 interface, we introduced cysteine
4 residues at the base of the VgrG1 gp27 hub domain and at each side of the Hcp1 hexamer. We
5 reasoned that the thiol groups of cysteine side-chains would form disulfide bonds if located at
6 appropriate distances ($C\alpha$ - $C\alpha$ distance $< 7 \text{ \AA}$). We first performed molecular docking
7 simulations using the structure of Hcp1 [59] and the generated structural model of VgrG1.
8 Based on the best matches, cysteine residues were rationally positioned in loops, substituting
9 residues sharing a 3 to 7- \AA $C\alpha$ - $C\alpha$ distance. Six positions were substituted on the cysteine-
10 less (C38S) Hcp1: Gln-24, Asn-46, Gly-48, Ala-95, Gly-96 and Ser-158. Gln-24, Ala-95 and
11 Gly-96 locate at the Hcp1 tail side whereas Asn-46, Gly-48 and Ser-158 locate at the Hcp1
12 head side. The Hcp1 Q24C, G48C, A95C, G96C, and S158C mutants were previously shown
13 to be functional [47]. The VgrG1 protein possesses five native cysteine residues, including
14 two in the gp27-like hub domain (Cys-27 and Cys-379). Because the bacterial cytoplasm is
15 considered as reducing, formation of disulfide bonds between the VgrG1 and Hcp1 cysteine
16 variants was catalyzed in presence of the oxidative agent copper(II) orthophenanthroline. Fig.
17 5A shows that none of the VgrG1 native cysteines engages in disulfide bond formation with
18 the Hcp1 cysteine variants. Thus, two residues located in the VgrG1 360-362 loop that is
19 important for VgrG1-Hcp1 complex formation were substituted by cysteines in the wild-type
20 VgrG1 protein: Arg-361 and Lys-362. Interbacterial competition assays demonstrated that the
21 Hcp1 N46C and VgrG1 R361C and K362C mutants are functional (Fig. S5). Fig. 5B shows
22 that higher molecular weight species (denoted with * and ** in the anti-VSV-G and anti-
23 FLAG immunoblots, respectively) are observable for four combinations involving VgrG1
24 R361C and K362C and Hcp1 N46C and G48C. The apparent molecular weight of these

1 species (~ 120 kDa) is compatible with a complex between VgrG1 (theoretical weight: 93
2 kDa) and Hcp1 (theoretical weight: 18 kDa). These complexes are likely to be covalently
3 bound by disulfide bridges as they dissociate upon addition of a reducing agent (Fig. 5C), and
4 likely comprise both VgrG1 and Hcp1 as they are recognized by both the VSV-G and FLAG
5 antibodies (Fig. 5D).

6

7 **DISCUSSION**

8 In this study, BACTH, co-IP, MST and disulfide bond cross-linking assays
9 demonstrated that the component of the T6SS inner tube, Hcp1, interacts with the needle
10 spike VgrG1 in EAEC. A complex comprising the *Agrobacterium tumefaciens* VgrG and Hcp
11 proteins has been previously reported using co-immunoprecipitation [41]. Interaction between
12 the VgrG spike and the Hcp tube component is likely to be conserved in all T6SS. Indeed,
13 additional results demonstrated that the Hcp and VgrG proteins associated with the EAEC
14 Sci-2 and *V. cholerae* T6SS gene clusters also interact. Interestingly, we also showed that
15 cross-interactions between non-cognate Hcp and VgrG proteins from the two EAEC T6SS
16 gene clusters exist, albeit with a significant decrease in affinity compared to cognate pairs.
17 However, *in vivo* studies showed that VgrG2 and Hcp2 cannot functionally replace VgrG1
18 and Hcp1, respectively.

19 Our VgrG1 deletion studies demonstrated that its gp27-like domain is sufficient to
20 interact with Hcp1. Interestingly, we showed that neither the gp5 OB-fold nor the β -helix or
21 the C-domains are essential for the assembly for the T6SS apparatus since the gp27 domain is
22 sufficient to promote Hcp1 assembly, sheath extension and contraction, and Hcp1 release in
23 the milieu. In addition, a previous report from our laboratory had shown that the VgrG1 C-

1 terminal extension is necessary to cause target cell lysis by binding and delivering the Tle1
2 phospholipase effector [55]. Taken together, these information suggest that the VgrG1 gp27-
3 like hub is sufficient to promote assembly of the T6SS, and that the β -helix and C-terminal
4 extension are required to penetrate the cell envelope of the target cell and to deliver effectors.
5 The observation that Hcp1 is released in the medium of cells producing the VgrG1 gp27-like
6 domain further suggests that the VgrG1 β -helix is not required for piercing the outer
7 membrane of the producing cell, and therefore that the needle should cross the outer
8 membrane through a dedicated channel such as that proposed by a conformational change of
9 the outermost portion of the TssJLM complex [11]. Our data also showed that the VgrG1 OB-
10 fold domain is not necessary for promoting Hcp1 tube formation, which is in agreement with
11 the suggestion that the OB-fold acts as a symmetry connector between the six-fold gp27-like
12 hub domain and the three-fold β -helix needle domain [38].

13 Mutational studies and docking simulations coupled to disulfide bond assays detailed
14 the contacts between Hcp1 and VgrG1 (Fig. 6). Using substitutions with tryptophan, a bulky
15 side-chain aminoacid, we showed that the head side of the Hcp1 hexameric ring mediates
16 contacts with the gp27-like base of VgrG1. In agreement with this organization, the opposite
17 side of Hcp engages contacts with TssA, a subunit that coordinates the assembly of the inner
18 tube with the polymerization of the sheath and that remains associated with the distal end of
19 the tail during its extension [53]. Formation of disulfide bonds between cysteine residues
20 located at positions 46 and 48 of Hcp1 and 361 and 362 of VgrG1 allows to propose a model
21 for Hcp1 binding to VgrG1 (Fig. 6).

22 Interestingly, Leiman et al. noted that the gp27-like domain of the VgrG trimer has a
23 fold similar to that of an Hcp hexamer [38]. When superimposed, the VgrG basal side
24 corresponds to the tail side of Hcp. By interacting with the Hcp1 head side, VgrG1 engages

1 into a head-to-tail organization with Hcp1, and hence in an association comparable to that
2 between two Hcp1 hexamers. We thus propose that the hub formed by the VgrG gp27-like
3 domain trimer serves as an adaptor to recruit the first Hcp hexameric ring and thus initiates
4 the assembly of the inner tube. In agreement with this proposal, *in vivo* tube formation assays
5 have shown that the Hcp1 tube does not assemble properly in absence of *vgrG1* [47].
6 Interestingly, affinity measurements demonstrate that Hcp proteins interact with their cognate
7 VgrG with a K_D in the 1-10 micromolar range. With a K_D of $\sim 3 \mu\text{M}$, the affinity of Hcp1 for
8 VgrG1 is comparable - albeit better - to Hcp1 hexamers association ($7 \mu\text{M}$) [59]. Based on the
9 slightly better affinity for VgrG1, we propose that an Hcp1 hexamer binds to the free base of
10 VgrG1, which then becomes unavailable. Hcp1 tube polymerization can then proceed by the
11 addition of new Hcp1 hexamers on each other at the distal end of the growing structure (Fig.
12 7). This model agrees with recent data showing that the tail extends by the distal end [51, 53]

13

14 MATERIAL AND METHODS

15 **Bacterial strains, medium, and growth conditions.** Strains used in this study are listed in Table S1.
16 *Escherichia coli* DH5 α (New England Biolabs) was used for cloning procedures, W3110 for co-
17 immunoprecipitations, BTH101 [60] for bacterial two-hybrid assays and BL21(DE3)pLys (Invitrogen)
18 for protein purification. The enteroaggregative *E. coli* (EAEC) 17-2 strain and its $\Delta vgrG1$, $\Delta hcp1$,
19 $\Delta vgrG1\Delta hcp1$, and $\Delta vgrG1-tssB-mCh$ derivatives [12] have been used for *in vivo* studies. Cells were
20 routinely grown in Lysogeny broth (LB) at 30°C or 37°C. *sci-1* gene expression was induced in SIM
21 (Sci-1 inducing medium; M9 minimal medium supplemented with LB 10%, glycerol 0.4%,
22 casaminoacids 40 $\mu\text{g.mL}^{-1}$, MgCl_2 2 mM, CaCl_2 0.1 mM, Vitamin B1 200 $\mu\text{g.mL}^{-1}$) [61]. Terrific broth
23 (TB; 1.2% peptone, 2.4% yeast extract, 72 mM K_2HPO_4 , 17 mM KH_2PO_4 , and 0.4% glycerol) was
24 used for protein overproduction. Plasmids were maintained by addition of ampicillin (100 $\mu\text{g.mL}^{-1}$),
25 kanamycin (50 $\mu\text{g.mL}^{-1}$ for *E. coli* K-12; 100 $\mu\text{g.mL}^{-1}$ for EAEC) or chloramphenicol (40 $\mu\text{g.mL}^{-1}$).

1 Gene expression was induced with 0.1-0.5 mM isopropyl- β -thio-galactoside (IPTG) or L-arabinose
2 (0.02%).

3 **Plasmid construction.** Plasmids used in this study are listed in Table S1. Polymerase Chain Reactions
4 (PCR) were performed using a Biometra thermocycler using Pfu Turbo DNA polymerase (Agilent
5 Technology). Custom oligonucleotides, listed in Table S1, were synthesized by Sigma Aldrich. EAEC
6 17-2 chromosomal DNA was used as a template for all PCRs. *E. coli* strain DH5 α was used for
7 cloning procedures. Bacterial two-hybrid plasmids encoding T18 and T25 fusions to Hcp1 and VgrG1,
8 plasmid pBAD-VgrG1_V, encoding C-terminally VSV-G-tagged VgrG1 from the pBAD33 vector,
9 plasmids pUC-Hcp1_F and pUC-Hcp2_F, encoding N-terminally FLAG-tagged Hcp1 and Hcp2 from the
10 pUC12 vector, and plasmids pDest14-Hcp1 and pDest14-Hcp2, encoding Hcp1 and Hcp2 fused to a
11 C-terminal 6 \times His tag have been previously described [10, 42, 59, 62]. Plasmids encoding truncated
12 fragments of VgrG have been constructed by restriction/ligation-free cloning, as previously described
13 [62, 63]. Briefly, fragments of interest were amplified with oligonucleotides introducing extensions
14 annealing to the target vector. The double-stranded product of the first PCR has then been used as
15 oligonucleotides for a second PCR using the target vector as template. Except the N46C variant,
16 cysteine and tryptophan variants of Hcp1 have been previously described [47, 59]. Hcp1 N46C and
17 VgrG1 R361C, K362C and S360G-R361G-K362G (VgrG1_{loop}) substitutions have been introduced by
18 site-directed mutagenesis using complementary pairs of oligonucleotides and the Pfu Turbo high
19 fidelity polymerase (Agilent technologies). For protein purification, the DNA sequences encoding the
20 VgrG1 (VgrG1- Δ gp5, Met-1 to Asn-490), VgrG2 (VgrG2- Δ gp5, Met-1 to Asn-465) and *V. cholerae*
21 strain O395 VgrG (VgrG_{Vc}- Δ gp5, Met-1 to Gln-471) gp27/OB regions were amplified from EAEC 17-
22 2 or *V. cholerae* O395 and cloned into the pETG20A expression vector using standard Gateway
23 procedures to yield pETG20A-VgrG1- Δ gp5, pETG20A-VgrG2- Δ gp5, and pETG20A-VgrG_{Vc}- Δ gp5,
24 respectively. The resulting constructions allow the production of VgrG1- Δ gp5, VgrG2- Δ gp5, and
25 VgrG_{Vc}- Δ gp5 fused to an N-terminal thioredoxin followed by a 6 \times His tag and a Tobacco Etch Virus
26 (TEV) cleavage site. The DNA sequence encoding *V. cholerae* Hcp was amplified from strain O395

1 and cloned into the pDEST14 vector to yield pDest14-Hcp_{vc}. All constructs have been verified by
2 DNA sequencing (Eurofins).

3 ***In vivo* T6SS activity reporter assays.** The interbacterial competition assay has been performed as
4 described [55]. The Hcp release assay was performed as described [62] except that cells were grown
5 in SIM to absorbance at $\lambda=600$ nm (A_{600}) of 0.6. The periplasmic TolB marker was used as control for
6 cell integrity.

7 **Fluorescence microscopy.** Overnight cultures of EAEC 17-2 derivative strains were diluted 1:100 in
8 SIM medium and grown to an $A_{600} \sim 0.6$ to maximise the expression of the *sci-1* T6SS gene cluster
9 [61]. Cells were concentrated to an $A_{600} = 5$ in SIM, spotted on a thin pad of 1.5% agarose in SIM and
10 covered with a cover slip. Microscopy recordings and digital image processing have been performed
11 as previously described [42, 47, 53, 64]. The Z project (average intensity) plugin has been used to
12 merge and flatten all Z-planes. Microscopy analyses were performed at least three times, each with
13 technical triplicate, and a representative experiment is shown.

14 **Overproduction and purification of the EAEC Hcp and VgrG proteins.** *E. coli* BL21(DE3) pLysS
15 (Invitrogen) cells were transformed with the pDEST14 derivatives encoding Hcp proteins or
16 pETG20A derivatives encoding VgrG gp27/OB domains. Overnight cultures grown in TB
17 supplemented with ampicillin ($100 \mu\text{g.mL}^{-1}$) and chloramphenicol ($35 \mu\text{g.mL}^{-1}$) at 37°C were diluted
18 in TB and grown at 37°C to $A_{600} \sim 0.6$. The temperature was then decreased to 25°C and the
19 expression of the *hcp* or *vgrG* genes was induced with 500 mM IPTG for 18 h. Cells were harvested,
20 resuspended in buffer A (50 mM Tris-HCl (pH 8.0), 300 mM NaCl) supplemented with 1 mM of
21 EDTA, 0.5 mg.mL^{-1} of lysozyme, and phenylmethylsulfonyl fluoride (PMSF), submitted to three
22 freeze-thawing cycles and sonicated after the addition of $20 \mu\text{g.mL}^{-1}$ of DNase and 20 mM of MgCl_2 .
23 Insoluble material was discarded by centrifugation for 30 min at $16,000 \times g$. All the subsequent
24 purification steps were performed using an AKTA FPLC system. For Hcp proteins, the soluble
25 fraction was loaded onto a 5-mL HisTrap FF column (GE Health Sciences). After extensive washing,
26 the Hcp proteins were eluted in one step gradient of Imidazole 250 mM in Buffer A. For VgrG

1 proteins, we followed the same protocol used for Hcp proteins with additional purification steps.
2 Briefly, the soluble proteins purified after the first HisTrap purification step were desalted on a HiPrep
3 26/10 column (Sephadex™ G-25, Amersham Biosciences), and VgrG proteins were obtained by
4 cleavage using 2 mg of TEV protease for 18 h at 4°C and collected in the flow-through of a 5-mL
5 HisTrap FF column. The resulting soluble proteins were concentrated using the centricon technology
6 (Millipore, 10-kDa cut-off). After concentration, the soluble Hcp or VgrG proteins were passed
7 through a Sephadex 200 26/60 column pre-equilibrated with 25 mM Tris-HCl (pH7.5), 100 mM NaCl.

8 **Protein-protein interaction assays.** *Bordetella* adenylate cyclase-based bacterial two-hybrid [42], co-
9 immuno-precipitation [13] and oxidative cross-linking [47] experiments have been performed as
10 previously described. Microscale thermophoresis experiments were performed using a Monolith
11 NT.115 apparatus (NanoTemper). VgrG1-Δgp5, VgrG2-Δgp5 and VgrG_{Vc}-Δgp5 were labeled with the
12 blue-fluorescent dye NT-495-NHS (NanoTemper) and the buffer was exchanged for the assay buffer
13 (25 mM Tris-HCl (pH 7.5), 200 mM NaCl, glycerol 5%, 0.05% Tween-20) using a Nap5 column (GE
14 Healthcare). Titrations were conducted with a constant 200 nM fluorophore-labeled VgrG protein
15 solution against up to 600 μM of Hcp proteins. Each data point was measured in triplicate. Single-site
16 fitting was performed using the NanoTemper data analysis software.

17 **Protein modeling and molecular docking simulations.** The available structure of full-length VgrG1
18 protein from *P. aeruginosa* (PDB: 4MTK [Sycheva, Shneider and Leiman, unpublished] and 4UHV
19 [43]; 25.5/58.4% identity/similarity with EAEC VgrG1) was used as template to generate a model of
20 the full-length VgrG1 from EAEC using the Homology modeling server accessible from the WHAT
21 IF interactive interface. The HADDOCK2.2 webserver interface was used for molecular docking
22 simulations [65].

23 **Miscellaneous.** Sodium Dodecyl Sulfate-Poly Acrylamide Gel Electrophoresis (SDS-PAGE) was
24 performed using standard protocols. For immunostaining, proteins were transferred onto nitrocellulose
25 membranes, and immunoblots were probed with primary antibodies and goat secondary antibodies
26 coupled to alkaline phosphatase and were developed in alkaline buffer in presence of 5-bromo-4-

1 chloro-3-indolylphosphate and nitroblue tetrazolium. The anti-FLAG (clone M2, Sigma-Aldrich), and
2 anti-VSV-G (clone P5D4, Sigma-Aldrich) monoclonal antibodies, and alkaline phosphatase-
3 conjugated goat anti-mouse secondary antibodies (Beckman Coulter) have been purchased as
4 indicated and used as recommended by the manufacturer. The anti-TolB polyclonal antibody is from
5 our laboratory collection.

6

7 **ACKNOWLEDGEMENTS**

8 We thank the members of the Cascales, Cambillau, Llobès, Bouveret and Sturgis research groups for
9 insightful discussions, and Moly Ba, Isabelle Bringer, Annick Brun and Olivier Uderso for technical
10 assistance. This work was supported by the Aix-Marseille Université (AMU), the Centre National de
11 la Recherche Scientifique (CNRS) and grants from the Agence Nationale de la Recherche to E.C.
12 (ANR-10-JCJC-1303-03, ANR-14-CE14-0006-02 and ANR-17-CE11-0039-01). Undergraduate
13 laboratory works of M.G.R. and J.Z.B. were supported by the ANR-14-CE14-0006-02 and ANR-10-
14 JCJC-1303-03 grants, respectively. B.D. was supported by a Fondation pour la Recherche Médicale
15 (FRM) grant to C.C. (DEQ2011-0421282). A.Z. was supported by a doctoral fellowship from the
16 French Ministère de la Recherche and a FRM end-of-thesis fellowship (FDT20140931060). Y.R.B.
17 was supported by a doctoral fellowship from the French Ministère de la Recherche.

18

19 **REFERENCES**

- 20 [1] E. Cascales, The type VI secretion toolkit, *EMBO Rep.* 9 (2008) 735–741.
- 21 [2] J.M. Silverman, Y.R. Brunet, E. Cascales, J.D. Mougous, Structure and regulation of the type
22 VI secretion system, *Ann. Rev. Microbiol.* 66 (2012) 453–472.
- 23 [3] S.J. Coulthurst, The Type VI secretion system - a widespread and versatile cell targeting
24 system. *Res Microbiol.* 164 (2013) 640–654.

- 1 [4] N, Kapitein, A. Mogk, Deadly syringes: type VI secretion system activities in pathogenicity
2 and interbacterial competition, *Curr. Opin. Microbiol.* 16 (2013) 52–58.
- 3 [5] A.B. Russell, S.B. Peterson, J.D. Mougous, Type VI secretion system effectors: poisons with a
4 purpose, *Nat. Rev. microbiol.* 12 (2014) 137–148.
- 5 [6] E. Durand, C. Cambillau, E. Cascales, L. Journet, VgrG, Tae, Tle, and beyond: the versatile
6 arsenal of type VI secretion effectors, *Trends Microbiol.* 22 (2014) 498–507.
- 7 [7] J. Alcoforado Diniz, Y.C. Liu, S.J. Coulthurst, Molecular weaponry: diverse effectors
8 delivered by the type VI secretion system, *Cell. Microbiol.* 17 (2015) 1742–1751.
- 9 [8] F.R. Cianfanelli, L. Monlezun, S.J. Coulthurst, Aim, load, fire: the type VI secretion system, a
10 bacterial nanoweapon, *Trends Microbiol.* 24 (2016) 51–62.
- 11 [9] L.S. Ma, J.S. Lin, E.M. Lai, An IcmF family protein, ImpLM, is an integral inner membrane
12 protein interacting with ImpKL, and its walker a motif is required for type VI secretion
13 system-mediated Hcp secretion in *Agrobacterium tumefaciens*, *J Bacteriol.* 191 (2009) 4316–
14 4329.
- 15 [10] M.S. Aschtgen, M. Gavioli, A. Dessen, R. Lloubès, E. Cascales, The SciZ protein anchors the
16 enteroaggregative *Escherichia coli* type VI secretion system to the cell wall, *Mol. Microbiol.*
17 75 (2010) 886–899.
- 18 [11] E. Durand, V.S. Nguyen, A. Zoued, L. Logger, G. Péhau-Arnaudet, M.S. Aschtgen, S. Spinelli,
19 A. Desmyter, B. Bardiaux, A. Dujeancourt, A. Roussel, C. Cambillau, E. Cascales, R. Fronzes,
20 Biogenesis and structure of a type VI secretion membrane core complex, *Nature* 523 (2015)
21 555–560.
- 22 [12] Y.R. Brunet, A. Zoued, F. Boyer, B. Douzi, E. Cascales, The type VI secretion TssEFGK-VgrG
23 phage-like baseplate is recruited to the TssJLM membrane complex via multiple contacts and
24 serves as assembly platform for tail tube/sheath polymerization, *PLoS Genet.* 15 (3) (2015)
25 e1005545.
- 26 [13] A. Zoued, C.J. Cassaro, E. Durand, B. Douzi, A.P. España, C. Cambillau, L. Journet, E.
27 Cascales, Structure-function analysis of the TssL cytoplasmic domain reveals a new
28 interaction between the Type VI secretion baseplate and membrane complexes, *J Mol Biol.*
29 428 (2016) 4413–4423.

- 1 [14] L. Logger, M.S. Aschtgen, M. Guérin, E. Cascales, E. Durand, Molecular dissection of the
2 interface between the Type VI secretion TssM cytoplasmic domain and the TssG baseplate
3 component, *J Mol Biol.* 428 (2016) 4424–4437.
- 4 [15] V.S. Nguyen, L. Logger, S. Spinelli, P. Legrand, T.T. Huyen Pham, T.T. Nhung Trinh, Y.
5 Cherrak, A. Zoued, A. Desmyter, E. Durand, A. Roussel, C. Kellenberger, E. Cascales, C.
6 Cambillau, Type VI secretion TssK baseplate protein exhibits structural similarity with phage
7 receptor-binding proteins and evolved to bind the membrane complex, *Nat Microbiol.* 2
8 (2017) 17103.
- 9 [16] A. Zoued, Y.R. Brunet, E. Durand, M.S. Aschtgen, L. Logger, B. Douzi, L. Journet, C.
10 Cambillau, E. Cascales, Architecture and assembly of the type VI secretion system, *Biochim.*
11 *Biophys. Acta* 1843 (2014) 1664–1673.
- 12 [17] B.T. Ho, T.G. Dong, J.J. Mekalanos, A view to a kill: the bacterial Type VI secretion system,
13 *Cell Host Microbe* 15 (2014) 9–21.
- 14 [18] P.F. Sarris, E.D. Ladoukakis, N.J. Panopoulos, E.V. Scoulica, A phage tail-derived element
15 with wide distribution among both prokaryotic domains: a comparative genomic and
16 phylogenetic study. *Genome Biol Evol.* 6 (2014) 1739–1747.
- 17 [19] M. Basler, Type VI secretion system: secretion by a contractile nanomachine, *Philos. Trans. R.*
18 *Soc. Lond. Ser. B Biol. Sci.* 370 (2015) 1679.
- 19 [20] D. Böck, J.M. Medeiros, H.F. Tsao, T. Penz, G.L. Weiss, K. Aistleitner, M. Horn, M. Pilhofer,
20 In situ architecture, function, and evolution of a contractile injection system, *Science.* 357
21 (2017) 713-717.
- 22 [21] E. Cascales, Microbiology: and Amoebophilus invented the machine gun!, *Curr Biol.* 27
23 (2017) 1170–1173.
- 24 [22] P.G. Leiman, M.M. Shneider, Contractile tail machines of bacteriophages, *Adv. Exp. Med.*
25 *Biol.* 726 (2012) 93–114.
- 26 [23] G. Bönemann, A. Pietrosiuk, A. Mogk, Tubules and donuts: a type VI secretion story, *Mol*
27 *Microbiol.* 76 (2010) 815–821.

- 1 [24] J.B. Heymann, J.D. Bartho, D. Rybakova, H.P. Venugopal, D.C. Winkler, A. Sen, M.R. Hurst,
2 A.K. Mitra, Three-dimensional structure of the toxin-delivery particle antifeeding prophage
3 of *Serratia entomophila*, *J Biol Chem.* 288 (2013) 25276–25284.
- 4 [25] Y. Michel-Briand, C. Baysse, The pyocins of *Pseudomonas aeruginosa*, *Biochimie* 84 (2002)
5 499–510.
- 6 [26] N.J. Shikuma, M. Pilhofer, G.L. Weiss, M.G. Hadfield, G.J. Jensen, D.K. Newman, Marine
7 tubeworm metamorphosis induced by arrays of bacterial phage tail-like structures, *Science*
8 343 (2014) 529–533.
- 9 [27] T. Penz, M. Horn, S. Schmitz-Esser, The genome of the amoeba symbiont "Candidatus
10 *Amoebophilus asiaticus*" encodes an *afp*-like prophage possibly used for protein secretion,
11 *Virulence* 1 (2010) 541–545.
- 12 [28] M. Brackmann, S. Nazarov, J. Wang, M. Basler, Using force to punch holes: mechanics of
13 contractile nanomachines, *Trends Cell Biol.* 27 (2017) 623–632.
- 14 [29] T. Jank, S. Eckerle, M. Steinemann, C. Trillhaase, M. Schimpl, S. Wiese, D.M. van Aalten,
15 W. Driever, K. Aktories, Tyrosine glycosylation of Rho by *Yersinia* toxin impairs blastomere
16 cell behaviour in zebrafish embryos, *Nat Commun.* 6 (2015) 7807.
- 17 [30] A. Hachani, T.E. Wood, A. Filloux, Type VI secretion and antihost effectors, *Curr. Opin.*
18 *Microbiol.* 29 (2015) 81–93.
- 19 [31] C.R. Büttner, Y. Wu, K.L. Maxwell, A.R. Davidson, Baseplate assembly of phage Mu:
20 Defining the conserved core components of contractile-tailed phages and related bacterial
21 systems, *Proc Natl Acad Sci U S A.* 113 (2016) 10174–10179.
- 22 [32] F. Arisaka, M.L. Yap, S. Kanamaru, M.G. Rossmann, Molecular assembly and structure of the
23 bacteriophage T4 tail, *Biophys Rev.* 8 (2016) 385–396.
- 24 [33] N.M. Taylor, N.S. Prokhorov, R.C. Guerrero-Ferreira, M.M. Shneider, C. Browning, K.N.
25 Goldie, H. Stahlberg, P.G. Leiman, Structure of the T4 baseplate and its function in triggering
26 sheath contraction, *Nature* 533 (2016) 346–352.
- 27 [34] N.R. Watts, D.H. Coombs, Structure of the bacteriophage T4 baseplate as determined by
28 chemical cross-linking, *J Virol.* 64 (1990) 143–154.

- 1 [35] S. Kanamaru, P.G. Leiman, V.A. Kostyuchenko, P.R. Chipman, V.V. Mesyanzhinov, F.
2 Arisaka, M.G. Rossmann, Structure of the cell-puncturing device of bacteriophage T4, *Nature*
3 415 (2002) 553–557.
- 4 [36] F. Arisaka, S. Kanamaru, Protein interactions in the assembly of the tail of bacteriophage T4,
5 *Biophys Rev.* 5 (2013) 79–84.
- 6 [37] S. Pukatzki, A.T. Ma, A.T. Revel, D. Sturtevant, J.J. Mekalanos, Type VI secretion system
7 translocates a phage tail spike-like protein into target cells where it cross-links actin, *Proc.*
8 *Natl. Acad. Sci. USA.* 104 (2007) 15508–15513.
- 9 [38] P.G. Leiman, M. Basler, U.A. Ramagopal, J.B. Bonanno, J.M. Sauder, S. Pukatzki, S.K.
10 Burley, S.C. Almo, J.J. Mekalanos, Type VI secretion apparatus and phage tail associated
11 protein complexes share a common evolutionary origin, *Proc. Natl. Acad. Sci. U. S. A.* 106
12 (2009) 4154–4159.
- 13 [39] P.G. Leiman, F. Arisaka, M.J. van Raaij, V.A. Kostyuchenko, A.A. Aksyuk, S. Kanamaru,
14 M.G. Rossmann, Morphogenesis of the T4 tail and tail fibers, *Virology* 7 (2010) 355.
- 15 [40] E. Cascales, C. Cambillau, Structural biology of type VI secretion systems, *Philos. Trans. R.*
16 *Soc. Lond. Ser. B Biol. Sci.* 367 (2012) 1102–1111.
- 17 [41] J.S. Lin, L.S. Ma, E.M. Lai, Systematic dissection of the agrobacterium type VI secretion
18 system reveals machinery and secreted components for subcomplex formation, *PLoS ONE.* 8
19 (2013) e67647.
- 20 [42] A. Zoued, E. Durand, C. Bebeacua, Y.R. Brunet, B. Douzi, C. Cambillau, E. Cascales, L.
21 Journet, TssK is a trimeric cytoplasmic protein interacting with components of both phage-
22 like and membrane anchoring complexes of the Type VI secretion system, *J. Biol. Chem.* 288
23 (2013) 27031–27041.
- 24 [43] M. Spínola-Amilibia, I. Davó-Siguero, F.M. Ruiz, E. Santillana, F.J. Medrano, A. Romero,
25 The structure of VgrG1 from *Pseudomonas aeruginosa*, the needle tip of the bacterial type VI
26 secretion system, *Acta Crystallogr D Struct Biol.* 72 (2016) 22–33.
- 27 [44] D. Veessler, C. Cambillau, A common evolutionary origin for tailed-bacteriophage functional
28 modules and bacterial machineries, *Microbiol Mol Biol Rev.* 75 (2011) 423–433.

- 1 [45] K. Uchida, P.G. Leiman, F. Arisaka, S. Kanamaru, Structure and properties of the C-terminal
2 β -helical domain of VgrG protein from *Escherichia coli* O157, *J Biochem.* 155 (2014) 173–
3 182.
- 4 [46] D. Unterweger, B. Kostiuk, S. Pukatzki, Adaptor proteins of Type VI secretion system
5 effectors, *Trends Microbiol.* 25 (2017) 8–10.
- 6 [47] Y.R. Brunet, J. Hénin, H. Celia, E. Cascales, Type VI secretion and bacteriophage tail tubes
7 share a common assembly pathway, *EMBO Rep.* 15 (2014) 315–321.
- 8 [48] L.G. Pell, V. Kanelis, L.W. Donaldson, P.L. Howell, A.R. Davidson, The phage lambda major
9 tail protein structure reveals a common evolution for long-tailed phages and the type VI
10 bacterial secretion system, *Proc Natl Acad Sci U S A.* 106 (2009) 4160–4165.
- 11 [49] J.D. Mougous, M.E. Cuff, S. Raunser, A. Shen, M. Zhou, C.A. Gifford, A.L. Goodman, G.
12 Joachimiak, C.L. Ordoñez, S. Lory, T. Walz, A. Joachimiak, J.J. Mekalanos, A virulence
13 locus of *Pseudomonas aeruginosa* encodes a protein secretion apparatus. *Science.* 312 (2006)
14 1526–1530.
- 15 [50] M. Kudryashev, R.Y. Wang, M. Brackmann, S. Scherer, T. Maier, D. Baker, F. DiMaio, H.
16 Stahlberg, E.H. Egelman, M. Basler, Structure of the type VI secretion system contractile
17 sheath, *Cell* 160 (2015) 952–962.
- 18 [51] A. Vettiger, J. Winter, L. Lin, M. Basler, The type VI secretion system sheath assembles at the
19 end distal from the membrane anchor, *Nat Commun.* 8 (2017) 16088.
- 20 [52] J. Wang, M. Brackmann, D. Castano-Diez, M. Kudryashev, K.N. Goldie, T. Maier, H.
21 Stahlberg, M. Basler, Cryo-EM structure of the extended type VI secretion system sheath-tube
22 complex, *Nat. Microbiol.* 2 (2017) 1507–1512.
- 23 [53] A. Zoued, E. Durand, Y.R. Brunet, S. Spinelli, B. Douzi, M. Guzzo, N. Flaugnatti, P. Legrand,
24 L. Journet, R. Fronzes, T. Mignot, C. Cambillau, E. Cascales, Priming and polymerization of a
25 bacterial contractile tail structure, *Nature* 531 (2016) 59–63.
- 26 [54] A. Zoued, E. Durand, Y.G. Santin, L. Journet, A. Roussel, C. Cambillau, E. Cascales, TssA:
27 The cap protein of the Type VI secretion system tail, *Bioessays.* 39 (2017) 262.
- 28 [55] N. Flaugnatti, T.T. Le, S. Canaan, M.S. Aschtgen, V.S. Nguyen, S. Blangy, C. Kellenberger,
29 A. Roussel, C. Cambillau, E. Cascales, L. Journet, A phospholipase A1 antibacterial Type VI

- 1 secretion effector interacts directly with the C-terminal domain of the VgrG spike protein for
2 delivery, *Mol Microbiol.* 99 (2016) 1099–1118.
- 3 [56] A.J. Gerc, A. Diepold, K. Trunk, M. Porter, C. Rickman, J.P. Armitage, N.R. Stanley-Wall,
4 S.J. Coulthurst, Visualization of the *Serratia* Type VI secretion system reveals unprovoked
5 attacks and dynamic assembly, *Cell Rep.* 12 (2015) 2131–2142.
- 6 [57] A. Vettiger, M. Basler, Type VI secretion system substrates are transferred and reused among
7 sister cells, *Cell.* 167 (2016) 99–110.
- 8 [58] E.R. Ballister, A.H. Lai, R.N. Zuckermann, Y. Cheng, J.D. Mougous, In vitro self-assembly of
9 tailorable nanotubes from a simple protein building block, *Proc. Natl. Acad. Sci. USA.* 105
10 (2008) 3733–3738.
- 11 [59] B. Douzi, S. Spinelli, S. Blangy, A. Roussel, E. Durand, Y.R. Brunet, E. Cascales, C.
12 Cambillau, Crystal structure and self-interaction of the Type VI Secretion tail-tube orotein
13 from Enteroaggregative *Escherichia coli*, *PLoS ONE* 9 (2014) e86918.
- 14 [60] G. Karimova, J. Pidoux, A. Ullmann, D. Ladant, A bacterial two-hybrid system based on a
15 reconstituted signal transduction pathway, *Proc. Natl. Acad. Sci. USA.* 95 (1998) 5752–5756.
- 16 [61] Y.R. Brunet, C.S. Bernard, M. Gavioli, R. Lloubes, E. Cascales, An epigenetic switch
17 involving overlapping *fur* and DNA methylation optimizes expression of a type VI secretion
18 gene cluster, *PLoS Genetics* 7 (2011) e1002205.
- 19 [62] M.S. Aschtgen, C.S. Bernard, S. De Bentzmann, R. Lloubès, E. Cascales, *SciN* is an outer
20 membrane lipoprotein required for type VI secretion in enteroaggregative *Escherichia coli*, *J.*
21 *Bacteriol.* 190 (2008) 7523–7531.
- 22 [63] F. van den Ent, J. Lowe, RF cloning: a restriction-free method for inserting target genes into
23 plasmids, *J. Biochem. Biophys. Meth.* 67 (2006) 67–74.
- 24 [64] Y.R. Brunet, L. Espinosa, S. Harchouni, T. Mignot, E. Cascales, Imaging type VI secretion-
25 mediated bacterial killing, *Cell Rep.* 3 (2013) 36–41.
- 26 [65] G.C.P. van Zundert, J.P. Rodrigues, M. Trellet, C. Schmitz, P.L. Kastiris, E. Karaca, A.S.J.
27 Melquiond, M. van Dijk, S.J. de Vries, A.M.J. Bonvin, The HADDOCK2.2 web server: user-
28 friendly integrative modeling of biomolecular complexes, *J Mol Biol.* 428 (2016) 720–725.

29

1

2 **Legend to Figures**

3

4 **Figure 1. Hcp1 interacts with VgrG1.** (A) Bacterial two-hybrid analysis. BTH101 reporter
5 cells producing the indicated proteins fused to the T18 and T25 domain of the *Bordetella*
6 adenylate cyclase were spotted on X-Gal-IPTG reporter LB agar plates. The blue color of the
7 colony reports interaction between the two partners. Controls include T18 and T25 fusions to
8 Pal and TolB, two proteins that interact but unrelated to the T6SS. (B and C) Co-
9 immunoprecipitation assay. Soluble lysates of *E. coli* cells producing the indicated proteins
10 (VgrG1_V, VSV-G-tagged VgrG1; Hcp1_F, FLAG-tagged Hcp1) were subjected to
11 immunoprecipitation with anti-FLAG (B) or anti-VSV-G (C) coupled beads. The total lysates
12 (T) and immunoprecipitated (IP) material were separated by 12.5% acrylamide SDS-PAGE
13 and immunodetected with anti-VSV-G (upper panel) and anti-FLAG (lower panel)
14 monoclonal antibodies. The position of VgrG1_V and Hcp1_F are indicated on the right.
15 Molecular weight markers (in kDa) are indicated on the left.

16

17 **Figure 2. The gp27-like base of VgrG1 is sufficient to mediate interaction with Hcp1.** (A)
18 Schematic representation of the EAEC VgrG1 architecture. The different domains are
19 represented with a color code (blue, gp27; red, OB-fold; green, gp5-C; grey, coiled-coil,
20 DUF2345 and TTR). The boundaries (in amino-acid) are indicated. The EAEC VgrG1 core
21 domain has been modelled based on the crystal structure of the *P. aeruginosa* VgrG1 (PDB:
22 4MTK). (B) Schematic representations of VgrG1 and the deletion constructs used in this
23 study. The color code is the same as in panel (A). (C) Co-immunoprecipitation assay. Soluble
24 lysates of *E. coli* cells producing the indicated VSV-G-tagged VgrG1 deletion variants and
25 FLAG-tagged Hcp1 (Hcp1_F) were subjected to immunoprecipitation with anti-FLAG-coupled

1 beads. The total lysates (T) and immunoprecipitated (IP) material were separated by 12.5%
2 acrylamide SDS-PAGE and immunodetected with anti-VSV-G (upper panel) and anti-FLAG
3 (lower panel) monoclonal antibodies. The position of Hcp1_F is indicated on the right whereas
4 positions of the VgrG1 variants are indicated by asterisks. Molecular weight markers (in kDa)
5 are indicated on left. (D) Microscale thermophoresis. *Left upper panel:* Coomassie blue
6 staining of the VgrG1-Δgp5 and Hcp1 purified proteins subjected to SDS-PAGE. Molecular
7 weight markers are indicated on left. *Right upper panel:* Thermophoretic time trace
8 recordings of the unlabeled Hcp1 titration (from 0.3 nM to 100 μM) to a constant amount of
9 fluorescently labeled VgrG1-Δgp5. The measured changes in the MST response (ΔF) were
10 plotted against the Hcp1 concentration to estimate the binding constant ($K_D = 2.8 \pm 0.1 \mu\text{M}$)
11 (lower panel).

12

13 **Figure 3. The gp27-like base of VgrG1 is sufficient to promote Hcp1 tube formation,**
14 **sheath dynamics and Hcp1 release.** (A) Hcp1 tube formation. Cytoplasmic extracts from
15 Δ*vgrG1* cells (left panel), or Δ*vgrG1* cells producing VgrG1 (*vgrG1*⁺, middle panel) or
16 VgrG1-ΔOB (ΔOB, right panel) and FLAG-tagged Hcp1 (-) or the indicated Hcp1 variants
17 reporting head-to-head (H-to-H, G48C), tail-to-tail (T-to-T, Q24C/A95C) or head-to-tail (H-
18 to-T, G96C/S158C) assemblies after *in vivo* oxidative treatment were analyzed by 12.5%-
19 acrylamide SDS-PAGE and immunodetected with the anti-FLAG monoclonal antibody.
20 Positions of the Hcp1 monomer (Hcp1_F) and oligomers (Hcp1_F*) are indicated on the right.
21 Molecular weight markers (in kDa) are indicated on the left. (B) Sheath dynamics. Time-lapse
22 recordings of Δ*vgrG1* cells carrying the empty pBAD33 vector (*vgrG1*), the pBAD33 vector
23 producing VgrG1 (*vgrG1*⁺) or VgrG1-ΔOB (*vgrG1*-ΔOB) and producing the TssB-mCherry
24 fusion were monitored for 150 sec. Sheath extension and contraction events are pointed using
25 open and close arrowheads respectively. Scale bar is 1 μM. Statistical analyses of sheath

1 dynamics are shown in Fig. S3. (C) Hcp1 release assay. FLAG-tagged Hcp1 (Hcp1_F) release
2 was assessed by separating total cell (C) and cell-free culture supernatant (SN) fractions from
3 5×10^8 $\Delta vgrG1$ cells carrying the empty pBAD33 vector (*vgrG1*), the pBAD33 vector
4 producing VgrG1 (*vgrG1*⁺) or VgrG1- Δ OB (*vgrG1*- Δ OB). Proteins were separated by 12.5%-
5 acrylamide SDS-PAGE and periplasmic TolB and Hcp1_F were immunodetected using anti-
6 TolB (upper panel) and anti-FLAG (lower panel) antibodies. Molecular weight markers (in
7 kDa) are indicated on the left.

8

9 **Figure 4. The head and tail sides of the Hcp1 hexamer engage contacts with VgrG1 and**
10 **TssA respectively.** (A) Bacterial two-hybrid analysis. BTH101 reporter cells producing the
11 indicated proteins and variants fused to the T18 and T25 domain of the *Bordetella* adenylate
12 cyclase were spotted on X-Gal-IPTG reporter LB agar plates. The blue color of the colony
13 reports interaction between the two partners. Controls include T18 and T25 fusions to Pal and
14 TolB, two proteins that interact but unrelated to the T6SS. (B) Co-immunoprecipitation assay.
15 Soluble lysates of *E. coli* cells producing the indicated proteins or protein variants were
16 subjected to immunoprecipitation with anti-FLAG-coupled beads. The total lysates (T) and
17 immunoprecipitated (IP) material were separated by 12.5% acrylamide SDS-PAGE and
18 immunodetected with anti-VSV-G (upper panel) and anti-FLAG (lower panel) monoclonal
19 antibodies. The position of VgrG1_V and Hcp1_F are indicated on the right. Molecular weight
20 markers (in kDa) are indicated on the left. (C) VgrG1-Hcp1 interface. The structural model of
21 the EAEC VgrG1 protein (dark grey) and the structure of the EAEC Hcp1 hexameric ring
22 (light grey; PDB: 4HKH) are shown, highlighting the locations of the Hcp1 tryptophan
23 substitutions (red, N93W variant; green, S158W variant) and of three VgrG1 loops (red, Ser-
24 115 to Asn-120; green, Pro-219 to Ser-229; cyan, Ser-360 to Lys-362) at the base of the VgrG
25 gp27-like hub domain. The faces of Hcp1 engaged in the interactions with VgrG1 and TssA

1 are indicated with arrows. (D) Bacterial two-hybrid analysis. BTH101 reporter cells
2 producing the indicated proteins and variants fused to the T18 and T25 domain of the
3 *Bordetella* adenylate cyclase were spotted on X-Gal-IPTG reporter LB agar plates. The blue
4 color of the colony reports interaction between the two partners. Controls include T18 and
5 T25 fusions to Pal and TolB, two proteins that interact but unrelated to the T6SS. (E) Hcp1
6 tube formation. Cytoplasmic extracts from $\Delta vgrG1$ cells producing the VgrG1_{loop} variant and
7 FLAG-tagged Hcp1 (-) or the indicated Hcp1 variants reporting head-to-head (H-to-H, G48C),
8 tail-to-tail (T-to-T, Q24C/A95C) or head-to-tail (H-to-T, G96C/S158C) assemblies after *in*
9 *vivo* oxidative treatment were analyzed by 12.5%-acrylamide SDS-PAGE and
10 immunodetected with the anti-FLAG monoclonal antibody. Positions of the Hcp1 monomer
11 (Hcp1_F) and oligomers (Hcp1_F^{*}) are indicated on the right. Molecular weight markers (in kDa)
12 are indicated on the left. (F) *E. coli* K-12 recipient cells (W3110 *gfp*⁺, kan^R) were mixed with
13 the indicated attacker cells (WT, EAEC 17-2; $\Delta vgrG1$, $\Delta vgrG1$ cells carrying the pBAD33
14 empty vector; *vgrGI*⁺, $\Delta vgrG1$ cells producing VgrG1; *vgrGI*_{loop}, $\Delta vgrG1$ cells producing the
15 VgrG1_{loop} variant, spotted onto Sci-1 inducing medium (SIM) agar plates and incubated for 4
16 hours at 37°C. The image of a representative bacterial spot is shown below the graph
17 reporting the number of surviving *E. coli* prey cells (counted on selective kanamycin medium;
18 in log₁₀ of colony-forming units (cfu)). The open circles indicate values from three
19 independent assays, and the average is indicated by the bar.

20

21 **Figure 5. Disulfide bond formation between VgrG1 and Hcp1.** Cytoplasmic extracts from
22 cells producing the indicated VSV-G-tagged VgrG1 and FLAG-tagged Hcp1 cysteine variants
23 after *in vivo* oxidative treatment were subjected to 10%-acrylamide SDS-PAGE and
24 immunodetected with the anti-VSV-G (upper panels in panel A, B and C; "V" panels in panel
25 D) and anti-FLAG (lower panels in panel A, B and C; "F" panels in panel D) monoclonal

1 antibodies. In panel C, samples were treated (+) or not (-) with β -mercaptoethanol. In panel D,
2 each lane was cut vertically in two halves after protein transfer on nitrocellulose membrane
3 (dotted lines) and each half was immuno-detected with the anti-VSV-G (V) or anti-FLAG (F)
4 antibody. Positions of the Hcp1 (Hcp1_F) and VgrG1 (VgrG1_V) monomers, and of VgrG1-
5 Hcp1 complexes (* and **) are indicated on the right. Molecular weight markers (in kDa) are
6 indicated on the left.

7

8 **Figure 6. Model of the EAEC VgrG1-Hcp1 complex.** The modelled EAEC VgrG1 trimer
9 (same color code as Fig. 2A) is shown, as well as the Hcp1 hexameric ring (grey, PDB:
10 4HKH). VgrG1 and Hcp1 are docked based on the position of cysteine pairs that engage in
11 disulfide bond formation (Hcp1 N46C and G48C, yellow; VgrG1 R361C and K362C, purple).
12 A magnification is shown on right.

13

14 **Figure 7. Model for the early stages of T6SS tail biogenesis.** The assembly of the T6SS tail
15 tube/sheath starts after docking of the baseplate (BC) onto the membrane complex (MC) (1)
16 [11, 12]. The first ring of Hcp hexamer is recruited and docks to the VgrG base (2). Then,
17 Hcp hexameric rings and TssBC strands are recruited and the tail tube/sheath extends from
18 the distal end (3) [51, 53]. The VgrG protein is shown with the same color code as Fig. 2A
19 and Fig. 6. The tail tube/sheath coordinator TssA is shown in red. OM, outer membrane; PG,
20 peptidoglycan; IM, inner membrane.

21

22

1 Legend to Supplementary Figures

2

3 **Figure S1. Microscale thermophoresis affinity measurements between cognate and non-**

4 **cognate VgrG and Hcp proteins.** Thermophoretic time trace recordings of the unlabeled

5 EAEC Hcp1 or Hcp2, or *V. cholerae* Hcp (Hcp_{Vc}) titration (from 0.9 nM to 600 μM) to a

6 constant amount of fluorescently labeled EAEC VgrG1-Δgp5 or VgrG2-Δgp5 or *V. cholerae*

7 VgrG_{Vc}-Δgp5 (left panels). The measured changes in the MST response (ΔF) were plotted

8 against the Hcp concentration to calculate the binding constant (right panels). The VgrG2-

9 Δgp5 - Hcp2 (panel A, $K_D = 9.4 \pm 0.7 \mu\text{M}$), VgrG_{Vc}-Δgp5 - Hcp_{Vc} (panel B, $K_D = 4.1 \pm 0.4$

10 μM), VgrG1-Δgp5 - Hcp2 (panel C, $K_D = 35.4 \pm 6 \mu\text{M}$) and VgrG2-Δgp5 - Hcp1 (panel D,

11 $K_D = 22.4 \pm 1.9 \mu\text{M}$) recordings are shown.

12

13 **Figure S2. VgrG2 and Hcp2 do not compensate the absence of VgrG1 and Hcp1 for Sci1**

14 **T6SS-mediated inter-bacterial activity.** *E. coli* K-12 recipient cells (W3110 *gfp*⁺, *kan*^R)

15 were mixed with the indicated attacker cells: WT, EAEC 17-2; Δ*vgrG1*, Δ*vgrG1* cells

16 carrying the pBAD33 empty vector; *vgrG1*⁺, Δ*vgrG1* cells producing VgrG1; *vgrG2*⁺,

17 Δ*vgrG1* cells producing VgrG2 (panel A); WT, EAEC 17-2; Δ*hcp1*, Δ*hcp1* cells carrying the

18 pUC12 empty vector; *hcp1*⁺, Δ*hcp1* cells producing Hcp1; *hcp2*⁺, Δ*hcp1* cells producing

19 Hcp2 (panel B). The mixtures were spotted onto Sci-1 inducing medium (SIM) agar plates

20 and incubated for 4 hours at 37°C. The image of a representative bacterial spot is shown

21 below the graph reporting the number of surviving *E. coli* prey cells (counted on selective

22 kanamycin medium; in log₁₀ of colony-forming units (cfu)). The open circles indicate values

23 from three independent assays, and the average is indicated by the bar.

24

25

1 **Figure S3. Statistical analyses of sheath dynamics.** Distribution of the dynamic behavior of
2 T6SS sheaths, monitored by time-lapse fluorescence recordings of the indicated strain (WT,
3 EAEC 17-2; $\Delta vgrG1$, $\Delta vgrG1$ cells carrying the pBAD33 empty vector; $vgrG1^+$, $\Delta vgrG1$ cells
4 producing VgrG1; $vgrG1$ - Δ OB, $\Delta vgrG1$ cells producing VgrG1- Δ OB) producing the
5 chromosomally-encoded *tssB-mCherry* fusion. The bars represent the percentage of non-
6 dynamic tubular structures (blue) and sheaths that undergo cycles of extension-contraction
7 (green). The number of cells analysed (*n*) is indicated on top. The asterisk (*) indicates that no
8 sheath is observable in this strain (diffuse fluorescence).

9
10 **Figure S4. The gp27-like base of VgrG1 does not require VgrG2 to promote Hcp1**
11 **release.** FLAG-tagged Hcp1 (Hcp1_F) release was assessed by separating total cell (C) and
12 cell-free culture supernatant (SN) fractions from 5×10^8 $\Delta vgrG1$ - $\Delta vgrG2$ cells carrying the
13 empty pBAD33 vector (-), the pBAD33 vector producing VgrG1 ($vgrG1^+$), VgrG1- Δ OB
14 ($vgrG1$ - Δ OB) or VgrG2 ($vgrG2^+$). Proteins were separated by 12.5%-acrylamide SDS-PAGE
15 and periplasmic TolB and Hcp1_F were immunodetected using anti-TolB (upper panel) and
16 anti-FLAG (lower panel) antibodies. Molecular weight markers (in kDa) are indicated on the
17 left.

18
19 **Figure S5. Hcp1 and VgrG1 cysteine variants are functional for T6SS-dependent inter-**
20 **bacterial activity.** *E. coli* K-12 recipient cells (W3110 *gfp*⁺, kan^R) were mixed with the
21 indicated attacker cells (WT, EAEC 17-2; $\Delta hcp1$, $\Delta hcp1$ cells carrying the pUC12 empty
22 vector; *hcp1*⁺, $\Delta hcp1$ cells producing Hcp1; N46C, $\Delta hcp1$ cells producing the Hcp1 N46C
23 variant; $\Delta vgrG1$, $\Delta vgrG1$ cells carrying the pBAD33 empty vector; $vgrG1^+$, $\Delta vgrG1$ cells
24 producing VgrG1; R361C and K362C, $\Delta vgrG1$ cells producing the VgrG1 R361C and K362C
25 variants, respectively), spotted onto Sci-1 inducing medium (SIM) agar plates and incubated

1 for 4 hours at 37°C. The image of a representative bacterial spot is shown below the graph
2 reporting the number of surviving *E. coli* prey cells (counted on selective kanamycin medium;
3 in log₁₀ of colony-forming units (cfu)). The open circles indicate values from three
4 independent assays, and the average is indicated by the bar.

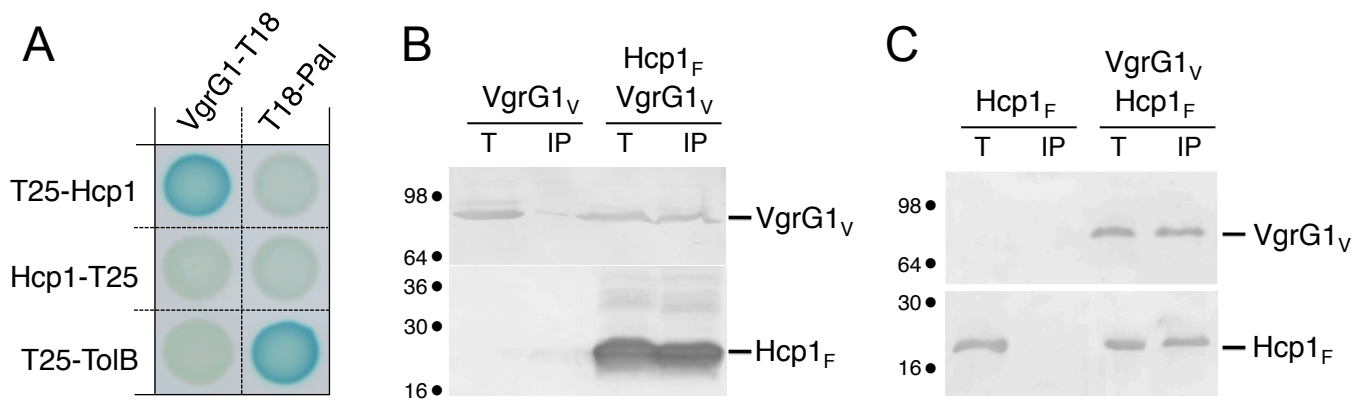


Figure 1

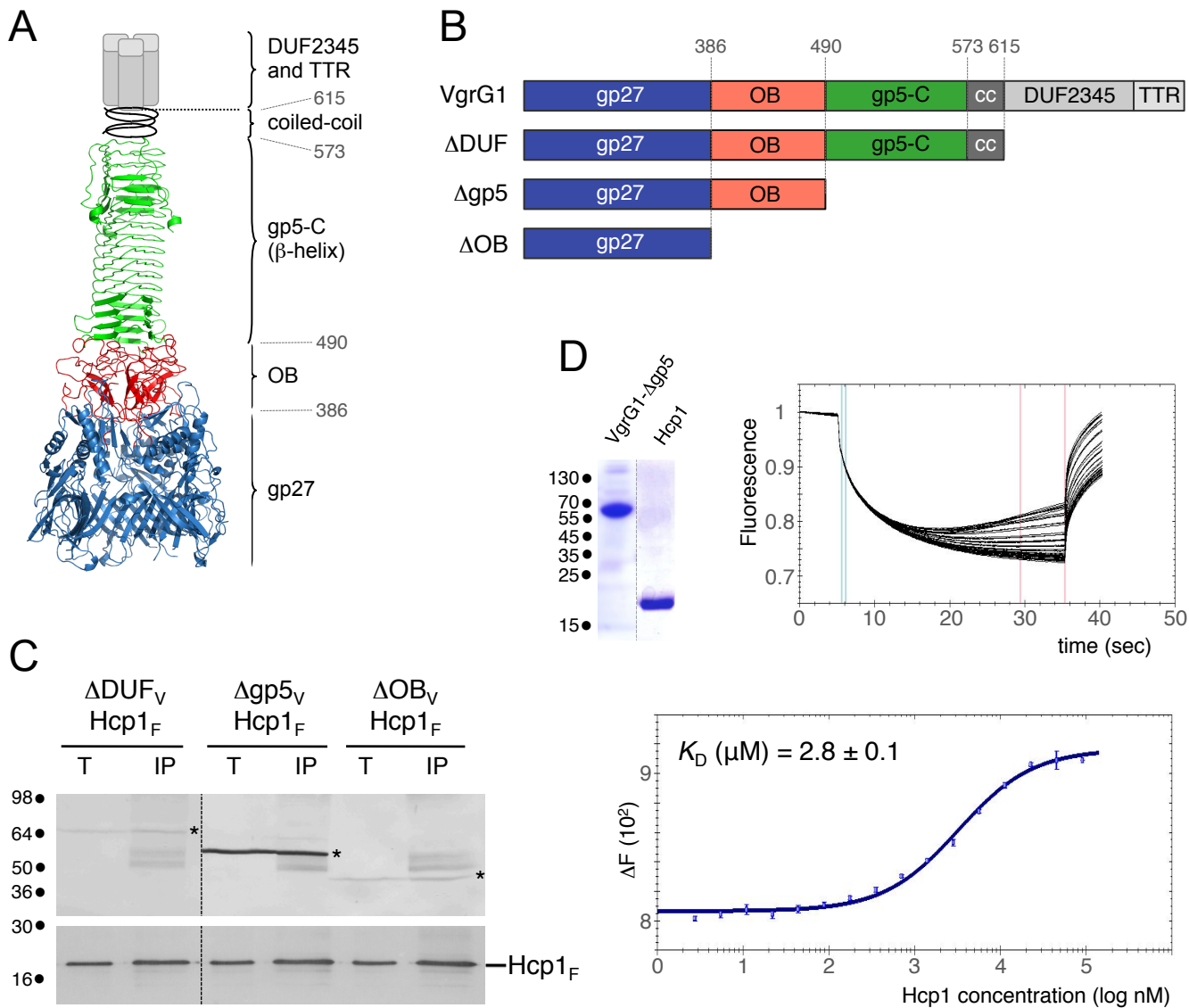


Figure 2

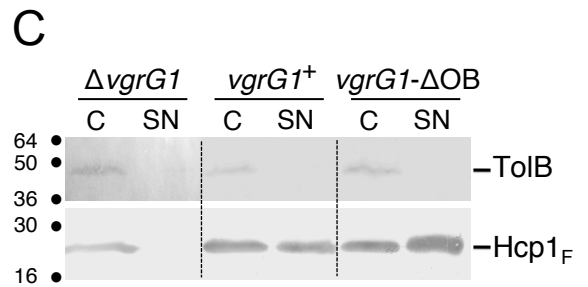
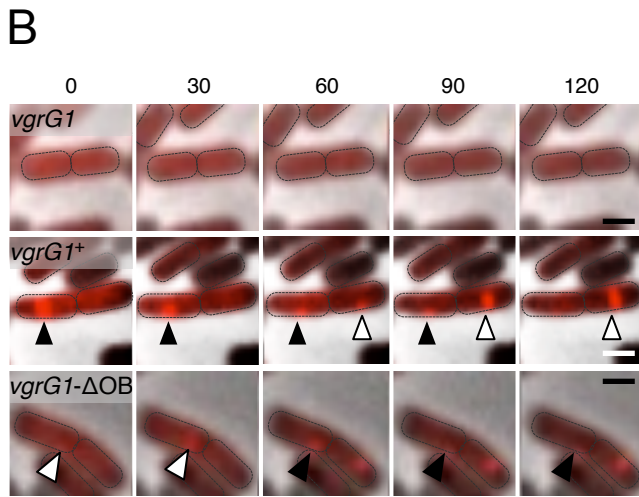
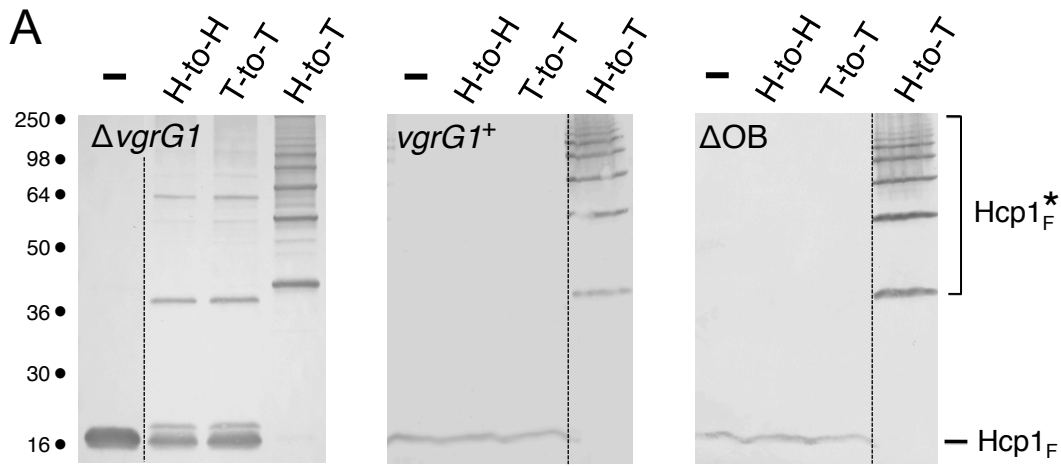


Figure 3

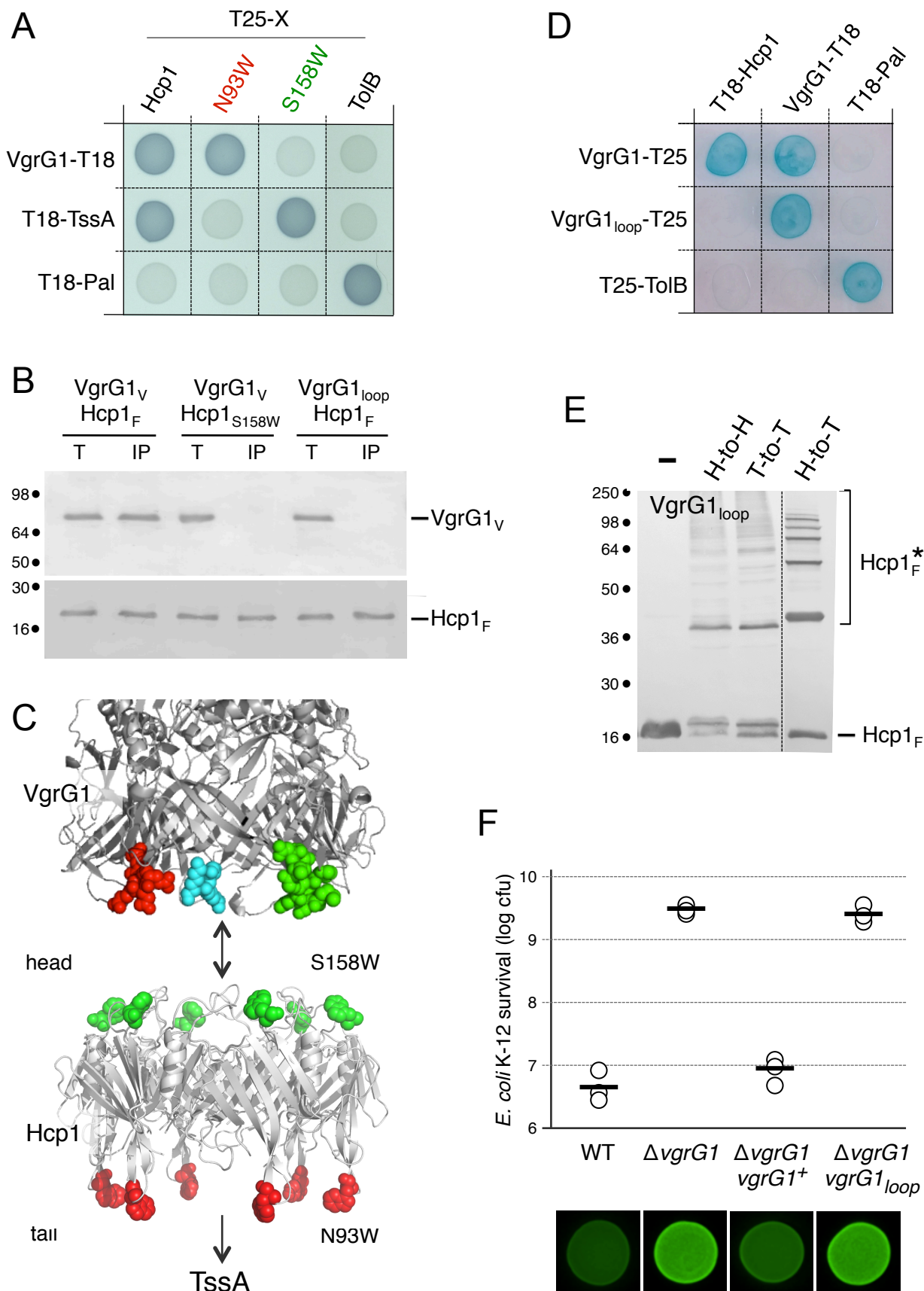


Figure 4

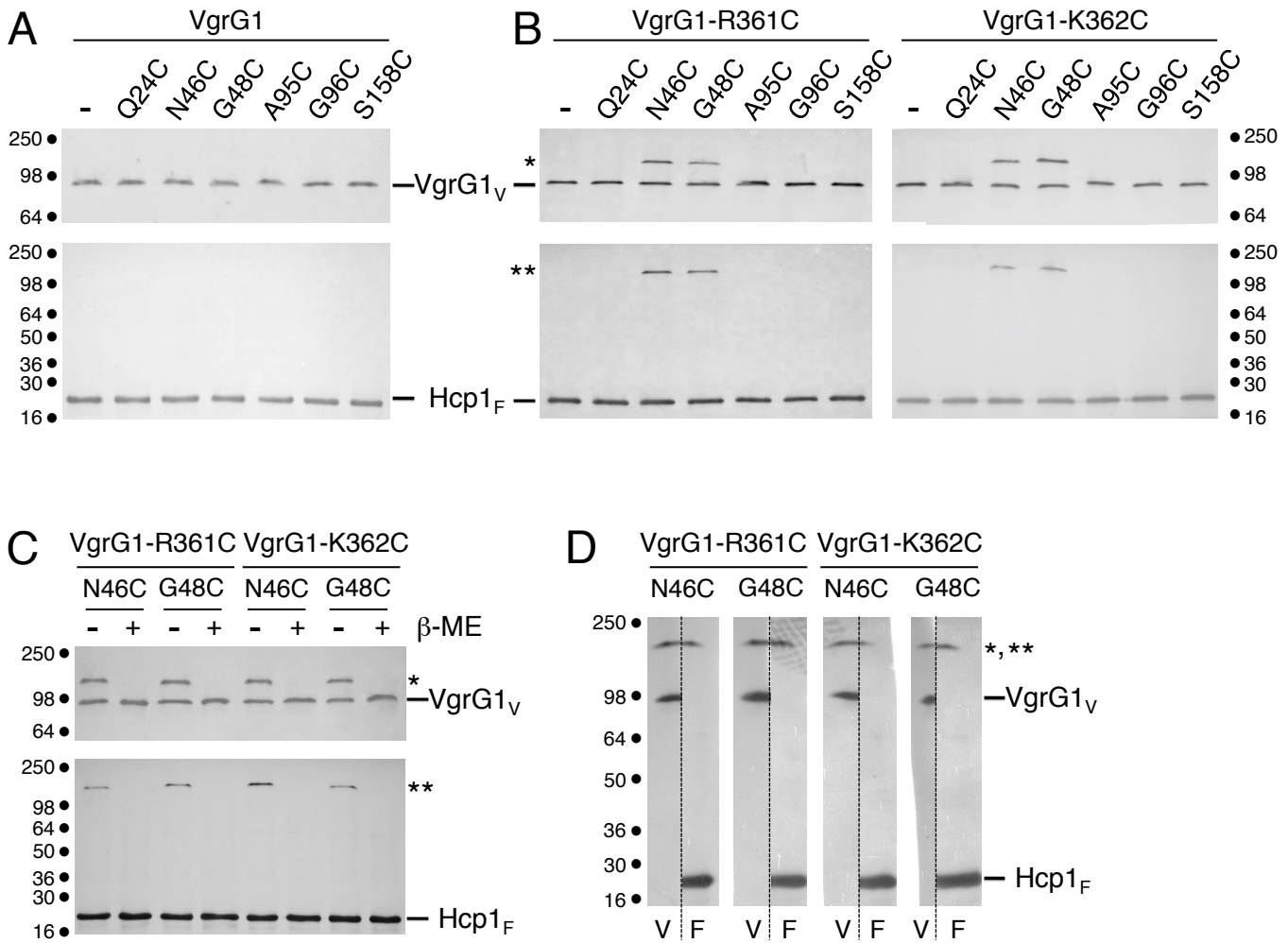


Figure 5

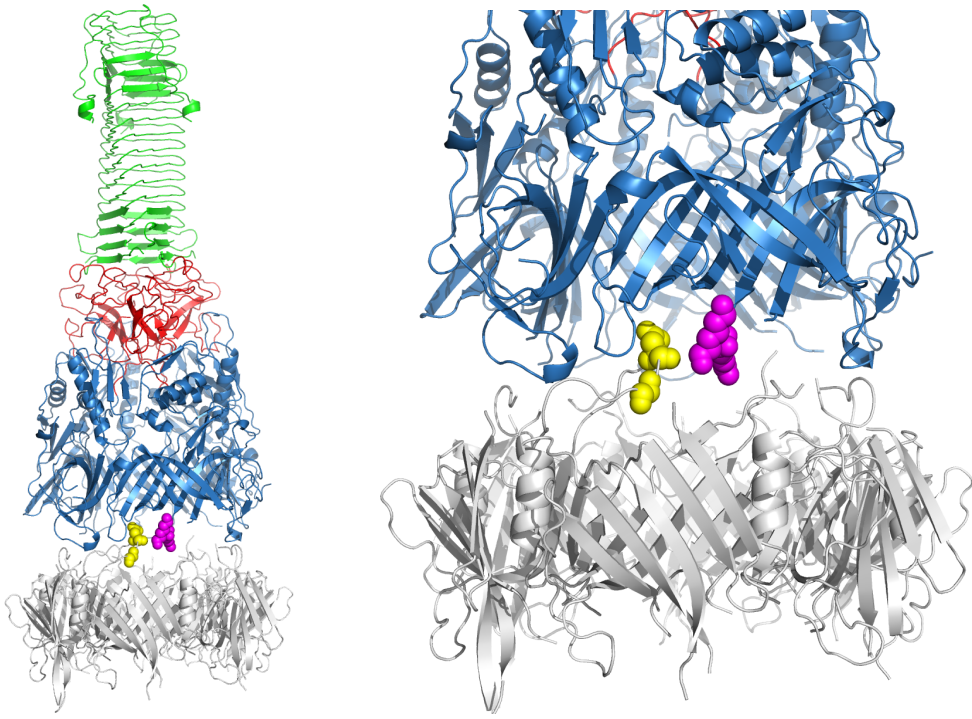
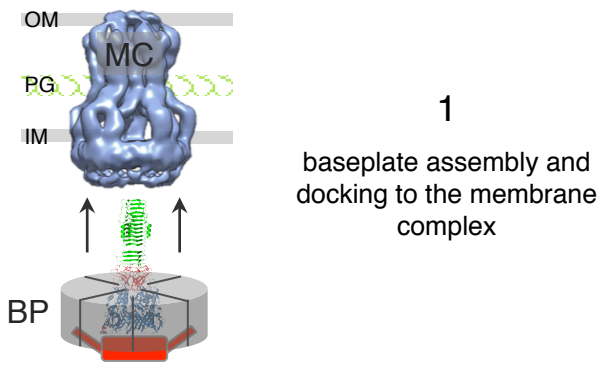
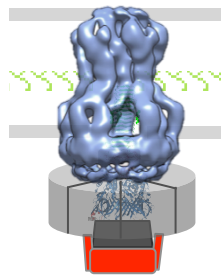
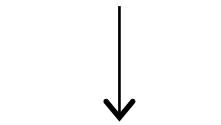


Figure 6



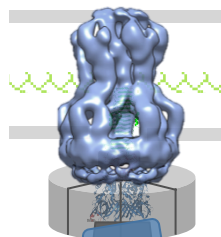
1

baseplate assembly and docking to the membrane complex



2

recruitment and interaction of the first Hcp ring to the VgrG base



3

coordinated polymerization of the inner tube and contractile sheath

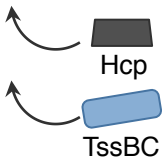


Figure 7

Table S1. Strains, plasmids and oligonucleotides used in this study.

STRAINS		
Strains	Description	Source/Reference
<u>Enteroaggregative <i>E. coli</i></u>		
17-2	Wild-type enteroaggregative <i>Escherichia coli</i>	A. Darfeuille-Michaud
$\Delta vgrG$	17-2 deleted of the <i>sci-1 vgrG</i> gene	Brunet <i>et al.</i> , 2014
Δhcp	17-2 deleted of the <i>sci-1 hcp</i> gene	Zhang <i>et al.</i> , 2013
$\Delta vgrG \Delta hcp$	$\Delta vgrG$ deleted of the <i>sci-1 hcp</i> gene	This study
$\Delta vgrG tssB-mCh$	$\Delta vgrG$ with mCherry inserted at the 3' of <i>tssB</i>	This study
<u><i>E. coli</i> K-12</u>		
DH5 α	F ⁻ , $\Delta(argF-lacZ)$ U169, <i>phoA</i> , <i>supE44</i> , $\Delta(lacZ)$ M15, <i>relA</i> , <i>endA</i> , <i>thi</i> , <i>hsdR</i>	New England Biolabs
BTH101	F ⁻ , <i>cya-99</i> , <i>araD139</i> , <i>galE15</i> , <i>galK16</i> , <i>rpsL</i> , <i>hsdR</i> , <i>mcrA1</i> , <i>mcrB1</i>	Karimova <i>et al.</i> , 1998
BL21(DE3)pLys	F ⁻ <i>ompT gal dcm lon hsdS_B(r_B⁻ m_B⁻)</i> λ (DE3) pLysS (Cm ^R)	Invitrogen
W3110	F ⁻ , λ IN(<i>rrnD-rrnE</i>)1 <i>rph-1</i>	Laboratory collection
PLASMIDS		
pETG20A	Amp ^R , ColE1, pT7, Gateway [®] destination vector, 6 \times His-TRX followed by a TEV cleavage site	Arie Gerlof
pET-VgrG1- Δ gp5	EAEC <i>sci-1 vgrG</i> (1-490) cloned upstream the TEV cleavage site into pETG20A	This study
pET-VgrG2- Δ gp5	EAEC <i>sci-2 vgrG</i> (1-465) cloned upstream the TEV cleavage site into pETG20A	This study
pET-VgrG _{Vc} - Δ gp5	<i>Vibrio cholerae</i> O395 <i>vgrG</i> (1-471) cloned upstream the TEV cleavage site into pETG20A	This study

pDEST14	Amp ^R , pBR322 ori, pT7, Gateway [®] destination vector, 6×His tag at C-terminus	Thermofisher
pDEST14-Hcp1	EAEC <i>sci-1 hcp</i> cloned into pDEST14	Douzi <i>et al.</i> , 2014
pDEST14-Hcp2	EAEC <i>sci-2 hcp</i> cloned into pDEST14	Douzi <i>et al.</i> , 2014
pDEST14-Hcp _{vc}	<i>Vibrio cholerae</i> O395 <i>hcp</i> cloned into pDEST14	This study
pEB354	Kan ^R , pKT25 derivative, P15A, Plac, T25 domain of <i>Bordetella</i> adenylate cyclase	Battesti & Bouveret, 2006
pEB355	Amp ^R , pUT18 derivative, ColE1, Plac, T18 domain of <i>Bordetella</i> adenylate cyclase	Battesti & Bouveret, 2006
pT18-Pal	<i>pal</i> cloned downstream T18 into pEB355	Battesti & Bouveret, 2006
pT25-TolB	<i>tolB</i> cloned downstream T25 into pEB354	Battesti & Bouveret, 2006
pT25-Hcp1	<i>sci-1 hcp</i> cloned downstream T25 into pEB354	Zoued <i>et al.</i> , 2013
pHcp1-T25	<i>sci-1 hcp</i> cloned upstream T25 into pEB354	Zoued <i>et al.</i> , 2013
pT25-Hcp1-N93W	Asn93-to-Trp substitution introduced into pT25-Hcp1	Brunet <i>et al.</i> , 2014
pT25-Hcp1-S158W	Ser158-to-Trp substitution introduced into pT25-Hcp1	Brunet <i>et al.</i> , 2014
pVgrG1-T18	<i>sci-1 vgrG</i> cloned upstream T18 into pEB355	Zoued <i>et al.</i> , 2013
pT18-TssA	<i>sci-1 tssA</i> cloned downstream T18 into pEB355	Zoued <i>et al.</i> , 2013
pT25-VgrG1	<i>sci-1 vgrG</i> cloned downstream T25 into pEB354	Zoued <i>et al.</i> , 2013
pT25-VgrG1loop	Ser360-to-Gly, Arg361-to-Gly and Lys362-to-Gly substitution introduced into pT25-VgrG1	This study
pBAD33	Cm ^R , P15A, pAraBAD, AraC, cloning vector.	Guzman <i>et al.</i> , 1995
pBAD-VgrG1	<i>sci-1 vgrG</i> fused to a C-terminal VSV-G tag cloned into pBAD33	This study
pBAD-VgrG1-ΔDUF	<i>sci-1 vgrG</i> (1-573) fused to a C-terminal VSV-G tag cloned into pBAD33	This study
pBAD-VgrG1-Δgp5	<i>sci-1 vgrG</i> (1-490) fused to a C-terminal VSV-G tag cloned into pBAD33	This study
pBAD-VgrG1-ΔOB	<i>sci-1 vgrG</i> (1-386) fused to a C-terminal VSV-G tag cloned into pBAD33	This study
pBAD-VgrG1-R361C	Arg361-to-Cys substitution introduced into pBAD-VgrG1	This study
pBAD-VgrG1-K362C	Lys362-to-Cys substitution introduced into pBAD-VgrG1	This study
pBAD-VgrG1loop	Ser360-to-Gly, Arg361-to-Gly and Lys362-to-Gly substitution introduced into pBAD-VgrG1	This study
pUC12	Amp ^R , ColE1, pLac, cloning vector	This study
pUC12-Hcp1	<i>sci-1 hcp</i> fused to a C-terminal FLAG tag cloned into pUC12	Aschtgen <i>et al.</i> , 2008
pUC12-Hcp2	<i>sci-2 hcp</i> fused to a C-terminal FLAG tag cloned into pUC12	Aschtgen <i>et al.</i> , 2008
pUC12-Hcp1-Q24C	Gln24-to-Cys substitution introduced into pUC12-Hcp1	Brunet <i>et al.</i> , 2014
pUC12-Hcp1-N46C	Asn46-to-Cys substitution introduced into pUC12-Hcp1	This study
pUC12-Hcp1-G48C	Gly48-to-Cys substitution introduced into pUC12-Hcp1	Brunet <i>et al.</i> , 2014
pUC12-Hcp1-A95C	Ala95-to-Cys substitution introduced into pUC12-Hcp1	Brunet <i>et al.</i> , 2014
pUC12-Hcp1-G96C	Gly96-to-Cys substitution introduced into pUC12-Hcp1	Brunet <i>et al.</i> , 2014
pUC12-Hcp1-S158C	Ser158-to-Cys substitution introduced into pUC12-Hcp1	Brunet <i>et al.</i> , 2014
pUC12-Hcp1-Q24C-A95C	Ala95-to-Cys substitution introduced into pUC12-Hcp1-Q24C	Brunet <i>et al.</i> , 2014
pUC12-Hcp1-G96C-S158C	Gly96-to-Cys substitution introduced into pUC12-Hcp1-S158C	Brunet <i>et al.</i> , 2014

OLIGONUCLEOTIDES

Insertion into pETG20A (Gateway cloning) ^{a, b}

VgrG1-Fwd	<u>GGGGACAAGTTTGTACAAAAAAGCAGGCTTACACCACCACCACCACCACGAAAACCTGTACTTCCAGGGTATGAATCT</u> CACTGACTCCCTGC
VgrG1-Δgp5-Rev	<u>GGACCACTTTGTACAAGAAAGCTGGGTCTTATTAGTTCTTATCGGTAACGTGATC</u>
VgrG2-Fwd	<u>GGGGACAAGTTTGTACAAAAAAGCAGGCTTACACCACCACCACCACCACGAAAACCTGTACTTCCAGGGTATGACTAG</u> GCAAAGATTTATATC
VgrG2-Δgp5-Rev	<u>GGACCACTTTGTACAAGAAAGCTGGGTCTTATTAATTATTCTCAGGAAGAGAAAAAG</u>
VgrG _{Vc} -Fwd	<u>ACAAAAAAGCAGGCTTACACCACCACCACCACCACGAAAACCTGTACTTCCAGGGTATGGCGACATTAGCGTACAGC</u>
VgrG _{Vc} -Δgp5-Rev	<u>GGACCACTTTGTACAAGAAAGCTGGGTCTTATTAGTGCTGAGGCAGGTGTATGGCGG</u>

Insertion into pDEST14 (Gateway cloning) ^{a, b}

Hcp1-Fwd	<u>GGGGACAAGTTTGTACAAAAAAGCAGGCTTAGAAGGAGATAGAACCATGAAAGCAATTCCAGTTTATCTGTG</u>
Hcp1-Rev	<u>GGGGACCACTTTGTACAAGAAAGCTGGGTTTATTAATGGTGATGGTGATGGTGCGCGGTGGTACGCTCACTCC</u>
Hcp2-Fwd	<u>GGGGACAAGTTTGTACAAAAAAGCAGGCTTAGAAGGAGATAGAACCATGAAAGTCGGAGTTATGAGTAATTC</u>
Hcp2-Rev	<u>GGGGACCACTTTGTACAAGAAAGCTGGGTTTATTAATGGTGATGGTGATGGTGACAAAGAGCCTCTTTATATAAG</u>
Hcp _{Vc} -Fwd	<u>GGGGACAAGTTTGTACAAAAAAGCAGGCTTAGAAGGAGATAGAACCCCACTCCATGTTATATCTCTATCG</u>
Hcp _{Vc} -Rev	<u>GGGGACCACTTTGTACAAGAAAGCTGGGTCTTAGTGATGGTGATGGTGATGCGCTTCGATTGGCTTACGCCAG</u>

Insertion into pBAD33 (restriction-free cloning) ^{a, c, d}

5-pBAD-VgrG	<u>CTCTCTACTGTTTCTCCATACCCGTTTTTTTTGGGCTAGCAGGAGGTATTACACCATGAATCTCACTGACTCCCTGCAAA</u> ATGTTTTATCC
3-pBAD-VgrG-573	<u>GGTCGACTCTAGAGGATCCCCGGGTACCTTATTTTCCTAATCTATTCATTTCAATATCTGTATACTTTCCTTGTGCCTGAGGC</u> TGCATATC
3-pBAD-VgrG-490	<u>GGTCGACTCTAGAGGATCCCCGGGTACCTTATTTTCCTAATCTATTCATTTCAATATCTGTATAACCGTTCTTATCGGTAACG</u> TGATCAACATGAC
3-pBAD-VgrG-386	<u>GGTCGACTCTAGAGGATCCCCGGGTACCTTATTTTCCTAATCTATTCATTTCAATATCTGTATAAGTAAGTAACGGTGGTCCG</u> CAGCAGAC

Site-directed mutagenesis ^e

A-Hcp1-N46C	TCTACATCCCGACGGATAACT <u>GT</u> ACCGGTAAGCTGACCGG
B-Hcp1-N46C	CCGGTCAGCTTACCGGTACAGTTATCCGTCGGGATGTAGA
A-VgrG1-R361C	AGCTTCTGTTACCGGTAGCTGTAATCTGCGCTACAGGT
B-VgrG1-R361C	ACCTGTAGCGCAGATTTACAGCTACCGGTGAACAGAAGCT
A-VgrG1-K362C	TTCTGTTACCGGTAGCCGGTGTCTGCGCTACAGGTGAT
B-VgrG1-K362C	ATCACCTGTAGCGCAGAACACCGGCTACCGGTGAACAGAA
A-VgrG1-loop	GCAGCTTCTGTTACCGGTGGCGGGGGATCTGCGCTACAGGTGATG
B-VgrG1-loop	CATCACCTGTAGCGCAGAT <u>CCCCCGCC</u> ACCGGTGAACAGAAGCTGC

^a sequence complementary to the pBAD33 plasmid (restriction-free cloning) or Gateway overhangs (Gateway cloning) underlined.

^b 6×His coding sequence in italics.

^c RBS and ATG sequence in bold.

^d VSV-G tag coding sequence in italics.

^e mutagenesized codon underlined.

Figure S1

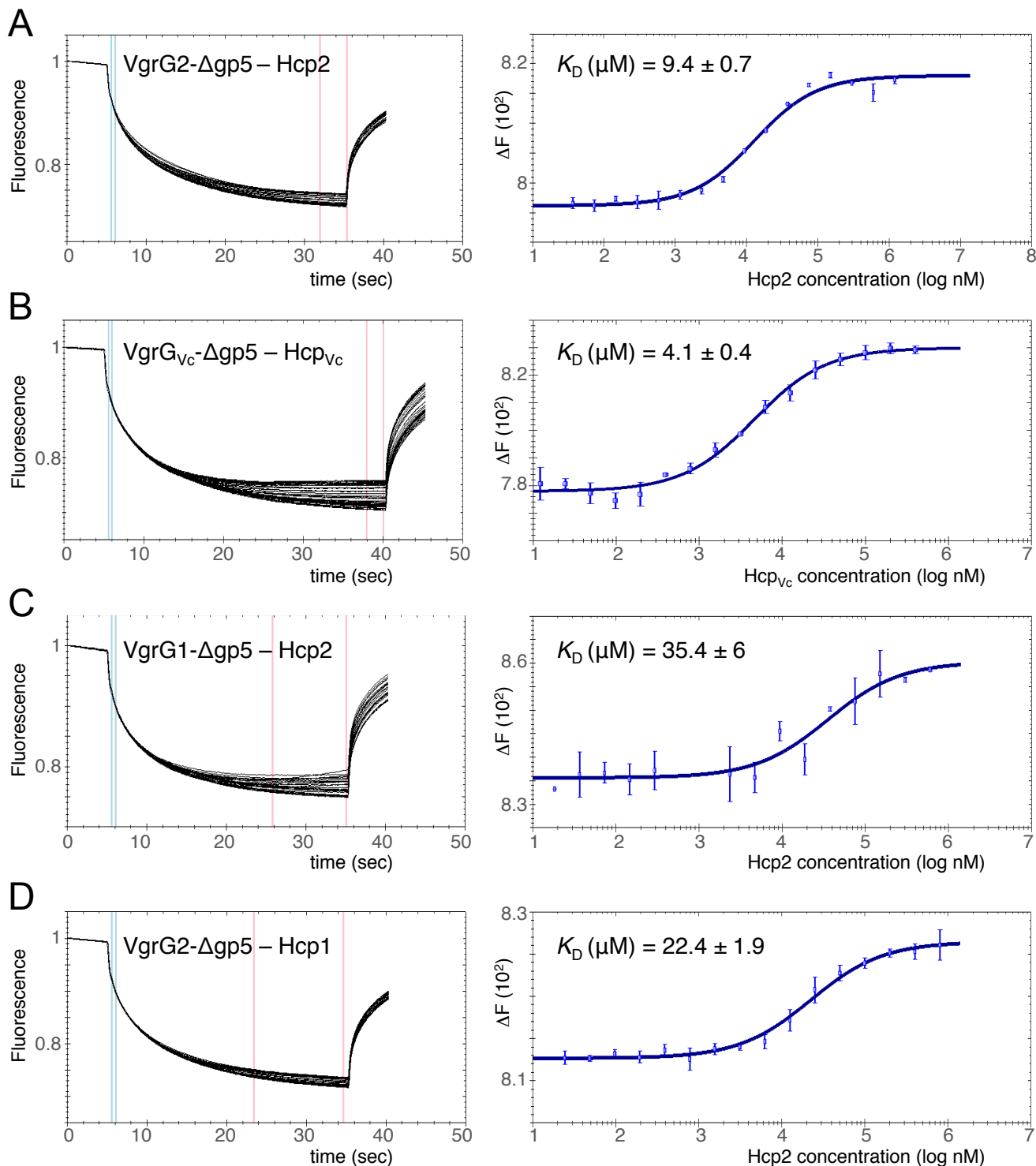


Figure S1. Microscale thermophoresis affinity measurements between cognate and non-cognate VgrG and Hcp proteins. Thermophoretic time trace recordings of the unlabeled EAEC Hcp1 or Hcp2, or *V. cholerae* Hcp (Hcp_{vc}) titration (from 0.9 nM to 600 μ M) to a constant amount of fluorescently labeled EAEC VgrG1- Δ gp5 or VgrG2- Δ gp5 or *V. cholerae* VgrG_{vc}- Δ gp5 (left panels). The measured changes in the MST response (ΔF) were plotted against the Hcp concentration to calculate the binding constant (right panels). The VgrG2- Δ gp5 - Hcp2 (panel A, $K_D = 9.4 \pm 0.7$ μ M), VgrG_{vc}- Δ gp5 - Hcp_{vc} (panel B, $K_D = 4.1 \pm 0.4$ μ M), VgrG1- Δ gp5 - Hcp2 (panel C, $K_D = 35.4 \pm 6$ μ M) and VgrG2- Δ gp5 - Hcp1 (panel D, $K_D = 22.4 \pm 1.9$ μ M) recordings are shown.

Figure S2

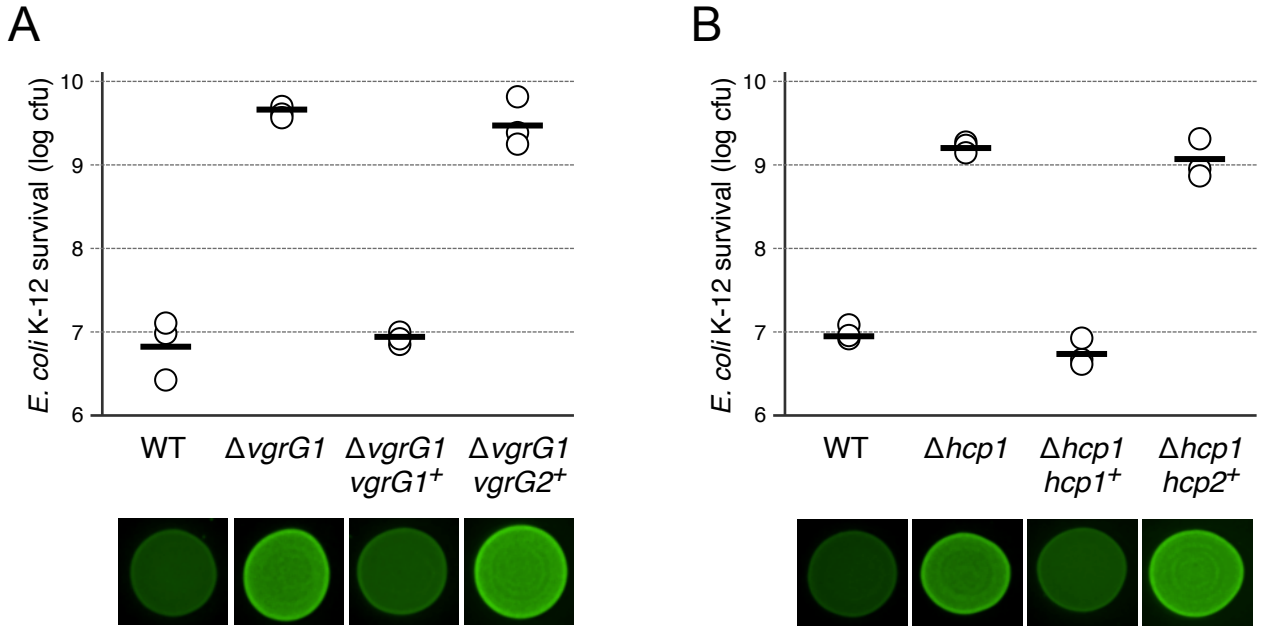


Figure S2. VgrG2 and Hcp2 do not compensate the absence of VgrG1 and Hcp1 for Sci1 T6SS-mediated inter-bacterial activity. *E. coli* K-12 recipient cells (W3110 *gfp*⁺, *kan*^R) were mixed with the indicated attacker cells: WT, EAEC 17-2; $\Delta vgrG1$, $\Delta vgrG1$ cells carrying the pBAD33 empty vector; *vgrG1*⁺, $\Delta vgrG1$ cells producing VgrG1; *vgrG2*⁺, $\Delta vgrG1$ cells producing VgrG2 (panel A); WT, EAEC 17-2; $\Delta hcp1$, $\Delta hcp1$ cells carrying the pUC12 empty vector; *hcp1*⁺, $\Delta hcp1$ cells producing Hcp1; *hcp2*⁺, $\Delta hcp1$ cells producing Hcp2 (panel B). The mixtures were spotted onto Sci-1 inducing medium (SIM) agar plates and incubated for 4 hours at 37°C. The image of a representative bacterial spot is shown below the graph reporting the number of surviving *E. coli* prey cells (counted on selective kanamycin medium; in log₁₀ of colony-forming units (cfu)). The open circles indicate values from three independent assays, and the average is indicated by the bar.

Figure S3

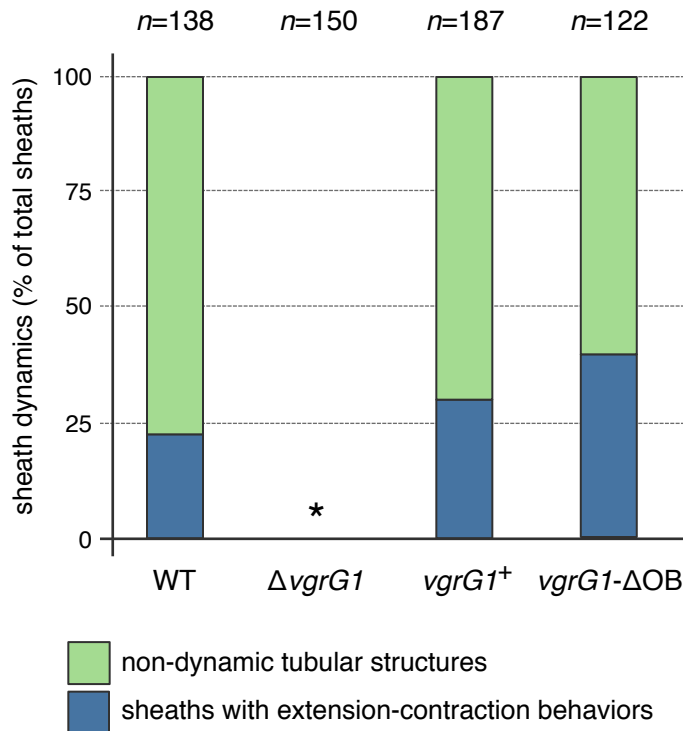


Figure S3. Statistical analyses of sheaths behavior. Distribution of the dynamic behavior of T6SS sheaths, monitored by time-lapse fluorescence recordings of the indicated strain (WT, EAEC 17-2; $\Delta vgrG1$, $\Delta vgrG1$ cells carrying the pBAD33 empty vector; $vgrG1^+$, $\Delta vgrG1$ cells producing VgrG1; $vgrG1-\Delta OB$, $\Delta vgrG1$ cells producing VgrG1- ΔOB) producing the chromosomally-encoded *tssB-mCherry* fusion. The bars represent the percentage of non-dynamic tubular structures (blue) and sheaths that undergo cycles of extension-contraction (green). The number of cells analysed (*n*) is indicated on top. The asterisk (*) indicates that no sheath is observable in this strain (diffuse fluorescence).

Figure S4

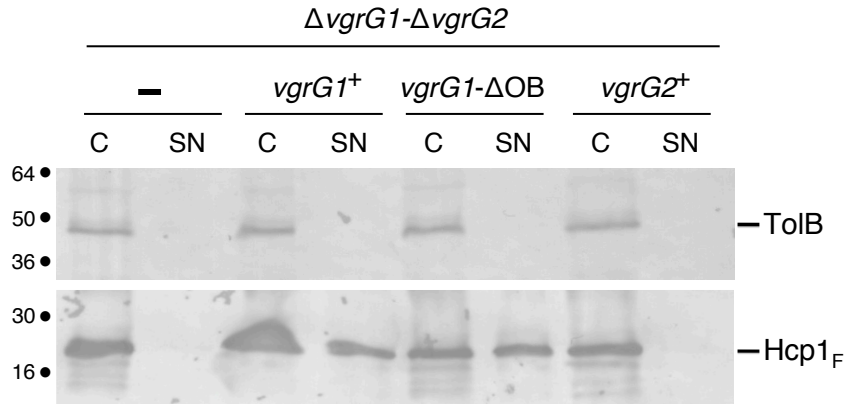


Figure S4. The gp27-like base of VgrG1 does not require VgrG2 to promote Hcp1 release. FLAG-tagged Hcp1 (Hcp1_F) release was assessed by separating total cell (C) and cell-free culture supernatant (SN) fractions from 5×10^8 $\Delta vgrG1-\Delta vgrG2$ cells carrying the empty pBAD33 vector (-), the pBAD33 vector producing VgrG1 (*vgrG1*⁺), VgrG1- Δ OB (*vgrG1*- Δ OB) or VgrG2 (*vgrG2*⁺). Proteins were separated by 12.5%-acrylamide SDS-PAGE and periplasmic TolB and Hcp1_F were immunodetected using anti-TolB (upper panel) and anti-FLAG (lower panel) antibodies. Molecular weight markers (in kDa) are indicated on the left.

Figure S5

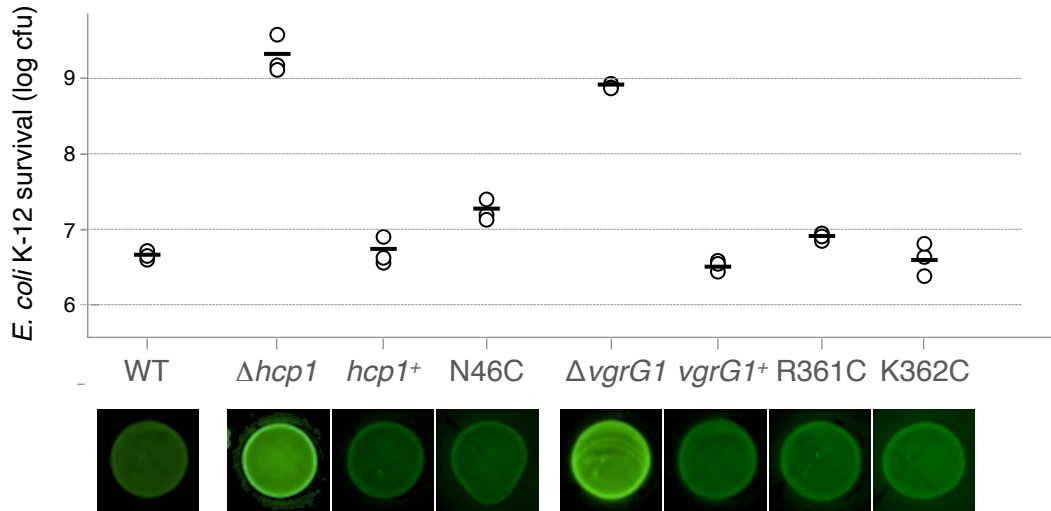


Figure S5. Hcp1 and VgrG1 cysteine variants are functional for T6SS-dependent inter-bacterial activity. *E. coli* K-12 recipient cells (W3110 *gfp*⁺, *kan*^R) were mixed with the indicated attacker cells (WT, EAEC 17-2; $\Delta hcp1$, $\Delta hcp1$ cells carrying the pUC12 empty vector; $hcp1^+$, $\Delta hcp1$ cells producing Hcp1; N46C, $\Delta hcp1$ cells producing the Hcp1 N46C variant; $\Delta vgrG1$, $\Delta vgrG1$ cells carrying the pBAD33 empty vector; $vgrG1^+$, $\Delta vgrG1$ cells producing VgrG1; R361C and K362C, $\Delta vgrG1$ cells producing the VgrG1 R361C and K362C variants, respectively), spotted onto Sci-1 inducing medium (SIM) agar plates and incubated for 4 hours at 37°C. The image of a representative bacterial spot is shown below the graph reporting the number of surviving *E. coli* prey cells (counted on selective kanamycin medium; in log₁₀ of colony-forming units (cfu)). The open circles indicate values from three independent assays, and the average is indicated by the bar.